Simulated changes in vegetation distribution, land carbon storage, and atmospheric CO_2 in response to a collapse of the North Atlantic thermohaline circulation

Peter Köhler[1,*], Fortunat Joos[2], Stefan Gerber[2,3], and Reto Knutti[2,4]

[1]Alfred Wegener Institute for Polar and Marine Research, PO Box 120161, D-27515 Bremerhaven, Germany
[*]Corresponding author: Phone: +49 471 4831 1687, Fax: +49 471 4831 1149, email: pkoehler@awi-bremerhaven.de
[2]Climate and Environmental Physics, Physics Institute, University of Bern, Sidlerstr. 5, 3012 Bern, Switzerland
[3]Now at: Princeton University, Princeton Forrestal Campus 201, Forrestal Road, PO Box 308, Princeton, NJ 08542-0308, USA
[4]Now at: National Center for Atmospheric Research, PO Box 3000, Boulder, CO 80307-3000, USA

Published in

Climate Dynamics, vol. 25 (7–8), p 689–708. DOI: 10.1007/s00382–005–0058–8, 2005

The original publication is available at www.springerlink.com.
Initial submission on 11 November 2004
Resubmission of final version on 2 June 2005
Accepted on 6 June 2005
Online First on 14 October 2005
http://dx.doi.org/10.1007/s00382-005-0058-8

Climate Dynamics, vol. 25 (7–8), p 689–708. DOI: 10.1007/s00382–005–0058–8, 2005 (2005) 0000:0001–28

Simulated changes in vegetation distribution, land carbon storage, and atmospheric CO_2 in response to a collapse of the North Atlantic thermohaline circulation

Peter Köhler[1,*], Fortunat Joos[2], Stefan Gerber[2,3], and Reto Knutti[2,4]

[1]Alfred Wegener Institute for Polar and Marine Research, PO Box 120161, D-27515 Bremerhaven, Germany
[*]Corresponding author: Phone: +49 471 4831 1687, Fax: +49 471 4831 1149, email: pkoehler@awi-bremerhaven.de
[2]Climate and Environmental Physics, Physics Institute, University of Bern, Sidlerstr. 5, 3012 Bern, Switzerland
[3]Now at: Princeton University, Princeton Forrestal Campus 201, Forrestal Road, PO Box 308, Princeton, NJ 08542-0308, USA
[4]Now at: National Center for Atmospheric Research, PO Box 3000, Boulder, CO 80307-3000, USA

Abstract. It is investigated how abrupt changes in the North Atlantic (NA) thermohaline circulation (THC) affect the terrestrial carbon cycle. The Lund-Potsdam-Jena Dynamic Global Vegetation Model is forced with climate perturbations from glacial freshwater experiments with the ECBILT-CLIO ocean-atmosphere-sea ice model. A reorganisation of the marine carbon cycle is not addressed. Modelled NA THC collapses and recovers after about a millennium in response to prescribed freshwater forcing. The initial cooling of several Kelvin over Eurasia causes a reduction of extant boreal and temperate forests and a decrease in carbon storage in high northern latitudes, whereas improved growing conditions and slower soil decomposition rates lead to enhanced storage in mid-latitudes. The magnitude and evolution of global terrestrial carbon storage in response to abrupt THC changes depends sensitively on the initial climate conditions. These were varied using results from time slice simulations with the Hadley Centre model HadSM3 for different periods over the past 21 kyr. Changes in terrestrial storage vary between -67 and $+50$ PgC for the range of experiments with different initial conditions. Simulated peak-to-peak differences in atmospheric CO_2 are 6 and 13 ppmv for glacial and late Holocene conditions. Simulated changes in δ^{13}C are between 0.15 and $0.25‰$. These simulated carbon storage anomalies during a NA THC collapse depend in their magnitude on the CO_2 fertilisation feedback mechanism. The CO_2 changes simulated for glacial conditions are compatible with available evidence from marine studies and the ice core CO_2 record. The latter shows multi-millennial CO_2 variations of up to 20 ppmv broadly in parallel with the Antarctic warm events A1 to A4 in the South and cooling in the North.

1 Introduction

Only few studies have addressed how a collapse of the North Atlantic (NA) thermohaline circulation (THC) might affect terrestrial vegetation distribution, the carbon cycle and atmospheric CO_2. However, knowledge on how changes in climate feed back on the atmospheric CO_2 concentration is required for reliable climate change projections.

The paleo proxy records of changes in climate, biogeochemical cycles and atmospheric CO_2 provide an important test-bed to evaluate climate-biogeochemical models. The models, in turn, are used to seek for mechanistic and quantitative explanation of environmental phenomena. The focus of this study is how changes in the NA THC such as those inferred for the last glacial period and projected in some global warming simulations affect vegetation distribution and terrestrial carbon stocks. The postulated link between changes in NA THC and terrestrial ecosystems is that a slow down or collapse of the formation of North Atlantic Deep Water (NADW) reduces northward heat transport in the Atlantic ocean, thereby modifying climate and, in turn, plant growth and soil decomposition in the NA region and beyond. This link is investigated by using results from freshwater perturbation experiments with the ECBILT-CLIO climate model to drive the Lund-Potsdam-Jena Dynamic Global Vegetation Model (LPJ-DGVM). Changes in vegetation distribution, carbon storage, and atmospheric CO_2 are assessed and discussed in the context of available proxy data and previous studies. A question raised is whether the model results are compatible with the ice CO_2 record and the evidence from available marine modelling studies.

The paleo records document large millennial scale climate variations during the last glacial period and the transition to the present interglacial. Greenland ice-core records show abrupt temperature changes locally of 10 K and more in amplitude (Johnsen et al., 1992, 1995; Lang et al., 1999; Landais et al., 2004) known as Dansgaard/Oeschger (D/O) events (Dansgaard et al., 1982; Oeschger et al., 1984, Fig. 1). Large temperature fluctuations in Greenland are also found for the onset and end of the Bølling/Allerød warm and the Younger Dryas (YD) cold phase during the transition. Isotopic sedimentary and pollen records from lakes, marine sediments and European and Asian loess records demonstrate that substantial effects of these abrupt climate changes extended over the

North Atlantic region and beyond (e.g. Voelker and workshop participants, 2002). A range of tracers indicative of water mass distribution and oceanic ventilation rates provide evidence that the NA THC was slowed or even collapsed during periods of cold temperatures in the NA region (e.g. McManus et al., 2004; Skinner and Shackleton, 2004). Some of the lowest temperatures in Greenland are associated with the surging of large amounts of ice, recorded as "Heinrich events" characterised by the widespread appearance of ice-rafted debris in North Atlantic sediments (Heinrich, 1988; Bond et al., 1993; Bond and Lotti, 1995; Rashid et al., 2003; Hemming, 2004, Fig. 1). Concomitant temperature changes recorded in Antarctica are smaller, less abrupt, and asynchronous to the northern hemisphere temperature changes (Jouzel et al., 2003; Blunier et al., 2004; Stenni et al., 2004, Fig. 1). The inter-hemispheric asynchrony ("bipolar seesaw") has been explained by a reduction in the North Atlantic Deep Water formation rate and oceanic heat transport into the North Atlantic region, producing cooling in the North Atlantic and warming in the Southern Hemisphere (Crowley, 1992; Broecker, 1998; Stocker, 1998) in combination with the large heat capacity of the Southern Ocean and sea level changes (Stocker and Johnsen, 2003; Knutti et al., 2004; Siddall et al., 2003). The Antarctic warm events associated with the stadials (cold periods) prior to the D/O (warm) events 8, 12, 14, and 17 are termed A1 to A4.

Despite the large fluctuations in climate, atmospheric CO_2 varied by only 20 ppmv during the Antarctic warm events associated with Heinrich events 4, 5, 5a, and 6 (Fig. 1, Stauffer et al., 1998; Indermühle et al., 2000). The 20 ppmv CO_2 peaks largely parallel the Antarctic warm events A1 to A4 and occur on a multi-millennial timescale. CO_2 rose by $\sim$20 ppmv in the YD cold interval (Monnin et al., 2001) during which the NA THC was significantly reduced (Sarnthein et al., 1994; McManus et al., 2004).

Many model experiments have been performed that address the response of the physical climate system to a NA THC collapse. Typically, the modelled NA THC is forced to collapse by imposing a freshwater discharge into the surface waters of the North Atlantic. Then, results are a strong cooling in the North Atlantic region spreading over the Northern Hemisphere and a slight warming in the Southern Hemisphere (e.g. Mikolajewicz, 1996; Timmermann et al., 2003; Knutti et al., 2004), consistent with proxy reconstructions.

The response of the carbon cycle and atmospheric CO_2 to past changes in the Atlantic meridional overturning circulation has only been partly addressed by modelling studies. Simulations with ocean carbon cycle models suggest that the changes in the marine carbon cycle associated with a NA THC collapse tend to increase atmospheric CO_2. Simulations with dynamic ocean models yield a small ($10 - 15$ ppmv) temporary increase in atmospheric CO_2 after the NA THC was forced to collapse by freshwater input (Marchal et al., 1998, 1999a,b). A recent ocean box model study (Köhler et al., 2005) suggests a small decrease in atmospheric CO_2 in response to a THC collapse, but ocean temperatures and marine export production were kept constant in the simulation.

These analyses did not consider the possible contribution from terrestrial sources to atmospheric CO_2. Terrestrial changes such as the replacement of extant boreal forests by steppe and tundra vegetation, a southward moving of the northern tree line, and a reduction in soil turnover rates in response to cooling may have contributed to the observed changes in atmospheric CO_2 concentration during the YD or the Antarctic warm events (Scholze et al., 2003b; Köhler and Fischer, 2004).

Scholze (2003) and Scholze et al. (2003b) found in their pioneering work a significant shift of the northern hemisphere vegetation distribution and the global carbon balance in response to a collapse and recovery of the NA THC. These authors forced the LPJ-DGVM with output from the ECHAM3/LSG atmosphere-ocean general circulation model. The global terrestrial carbon stock was reduced by about 180 PgC during the coldest phase in the Northern Hemisphere compared to the initial carbon stock in their standard experiment. The terrestrial release caused modelled atmospheric CO_2 to increase by 26 ppmv, taking into account the buffering by the ocean. Climatic input fields were perturbed from preindustrial conditions and the collapsed state of the THC extended over a few centuries.

Here, the role of a NA THC collapse on the terrestrial carbon balance, land ecosystems and atmospheric CO_2 and δ^{13}C was further investigated. As by Scholze et al. (2003b) and Scholze (2003), the spatio-temporal changes in vegetation distribution and terrestrial carbon storage were addressed using the LPJ-DGVM. Changes in atmospheric CO_2 and δ^{13}C were addressed in the framework of the Bern Carbon Cycle-Climate (BernCC) model that includes the LPJ-DGVM. In addition to Scholze and co-workers, climatic boundary conditions different to preindustrial conditions were applied. Initial conditions were varied systematically and the consequences of a NA THC collapse for glacial times, the glacial-interglacial transition, and the Holocene were investigated. A range of simulations was performed to investigate the sensitivity of model results to the abruptness and length of the NA THC collapse and to changes in the individual drivers (temperature, precipitation, ice extent, sea level, and atmospheric CO_2). Climate fields to drive the LPJ-DGVM model were taken from glacial freshwater experiments with the ECBILT-CLIO model (Knutti et al., 2004) that were run over several millennia and from time slice simulations with the Hadley Centre model HadSM3 covering various periods of the last 21 kyr.

The outline of this manuscript is as follows. First, the carbon cycle model, the climate models, the climate fields used to drive the LPJ-DGVM off-line, the model spin-up, and experimental protocols are described. In the subsection 3.1, results from freshwater discharge experiments with ECBILT-CLIO are summarised. In subsection 3.2, the carbon and vegetation distribution for preindustrial and for Last Glacial Maximum conditions are presented. Subsection 3.3 deals with the modelled impact of the NA THC changes on the terrestrial carbon cycle for preindustrial boundary condi-

tions. In subsection 3.4, the sensitivity of results to the initial climate conditions are investigated and in subsection 3.5 the sensitivity to the magnitude of the temperature perturbation is quantified. In the discussion and conclusion section, main results are summarised and discussed in the context of proxy data, available studies, and model limitations.

2 Methods

A version of the Bern Carbon Cycle-Climate Model (BernCC) was applied "off-line", similarly as by Joos et al. (2004), by forcing it with prescribed temperature, precipitation, and cloud cover fields. These climate fields were derived by combining (i) an observation-based climatology (Leemans and Cramer, 1991; New et al., 2000), (ii) anomalies from freshwater experiments with the ECBILT-CLIO model (Knutti et al., 2004), and (iii) anomalies from time slice simulations with the Hadley Centre model HadSM3 for different periods during the past 21 kyr (Table 1). The use of the Leemans and Cramer observation-based climatology ensures that LPJ-DGVM is driven by climatic fields that are as close as possible to reality. Interannual variations are essential to simulate fire in LPJ-DGVM and are derived here from observations by New et al. (2000). The ECBILT-CLIO anomaly fields represent the decadal-to-century scale climatic perturbations in response to a change in the NA THC. The HadSM3 anomaly fields represent the milllennial scale deviations in climate from the preindustrial state in response to slow changes in orbital parameters, greenhouse gas concentrations, and ice sheet extent. The HadSM3 anomalies were used to explore the sensitivity of results to different initial climate conditions. Existing observation-based and climate model data were applied in order that all available resources could be devoted to understanding terrestrial dynamics and their influence on the carbon cycle.

2.1 The Carbon Cycle Model

The carbon cycle model couples the LPJ-DGVM, the HIgh-Latitude exchange/interior Diffusion-Advection (HILDA) ocean carbon cycle model, and a well-mixed atmosphere.

LPJ-DGVM: The LPJ-DGVM (Sitch et al., 2003) was used to simulate changes in vegetation distribution and in the pools and fluxes of carbon and of the stable isotope ^{13}C (Scholze et al., 2003a). The LPJ-DGVM simulates photosynthesis, respiration, fire, and the growth and competition of nine plant functional types (PFT). PFT distributions are constrained by bioclimatic limits for plant survival and regeneration, while the relative performance of PFTs, in competition for light and water, is governed by PFT-specific physiological, phenological, growth and disturbance-response parameters. A PFT can invade new regions if its bioclimatic limits and competition with other PFTs allow successful establishment and growth. For each PFT, carbon is stored in seven pools, representing leaves, sapwood, heartwood, fine roots and litter compartments. Two soil organic matter pools receive input from the litter pools of all PFTs on each grid cell. Photosynthesis is modelled as a function of absorbed photosynthetically active radiation, temperature, atmospheric CO_2 concentrations, day length, canopy conductance, and biochemical pathway (C_3, C_4), using a simplified Farquhar scheme (Farquhar et al., 1980; Collatz et al., 1992), with leaf-level optimised nitrogen allocation (Haxeltine and Prentice, 1996) and an empirical convective boundary layer parameterisation (Monteith, 1995) to couple the carbon and water cycles. Fire fluxes are calculated based on litter moisture content, a fuel load threshold, and PFT specific fire resistances (Thonicke et al., 2001). Decomposition rates of soil organic matter and litter depend on soil temperature (Lloyd and Taylor, 1994) and moisture (Foley, 1995). The model is driven by atmospheric CO_2 and monthly fields of temperature, precipitation, and insolation (cloud-cover). The spatial resolution is set here to $3.75^\circ \times 2.5^\circ$. Due to a lack of adequate paleo soil data, the water holding capacity and thermal parameters of the soil were kept constant corresponding to the medium soil type with intermediate characteristics (one out of a set of nine soil types defined within the LPJ-DGVM). The choice of alternative soil types out of the common once for recent times would effects the steady state overall terrestrial carbon storage in a range of 50 PgC for preindustrial conditions.

The simulated potential natural vegetation (PNV) for preindustrial time (e.g. figure 12 in Joos et al., 2004) shows a generally good agreement with other global simulated PNV reconstructions (e.g. Cramer et al., 2001). The LPJ-DGVM predicts the high northern latitude greening trend over the past two decades observed by satellites and a marked setback in this trend after the Mount Pinatubo volcano eruption in 1991 (Lucht et al., 2002). The terrestrial carbon cycle as simulated by the LPJ-DGVM has been evaluated in combination with atmospheric transport models by comparing model results with observed seasonal cycle in atmospheric CO_2 (Sitch, 2000) and its temporal trend (McGuire et al., 2001; Dargaville et al., 2002) and by comparing the simulated time evolution and inter-annual variability of terrestrial carbon uptake with available reconstructions (McGuire et al., 2001), and shown to be compatible with these observations.

HILDA: The LPJ-DGVM was coupled to the HILDA ocean carbon cycle model (version K(z)) (Siegenthaler and Joos, 1992; Joos et al., 1996) as in previous studies (Joos et al., 2001, 2004; Gerber et al., 2003). HILDA is a box-diffusion type carbon cycle model that was developed to study the uptake of anthropogenic CO_2. Perturbation equations are used to calculate oceanic CO_2 uptake or release in response to an atmospheric CO_2 perturbation. The transport parameters were derived by tuning the model towards the observed oceanic distribution of natural and bomb-produced radiocarbon. The transport rates in HILDA have been evaluated using CFCs. Here, HILDA is used to calculate the physico-chemical buffering by the ocean of terrestrial carbon released to (removed from) the atmosphere. 64% and 85% of carbon released by the terrestrial pools will have been taken up by a preindustrial ocean after 100 and 1000 years, respec-

tively (see figure 1 in Joos et al., 2004). Ocean uptake rates for terrestrial carbon might have been somewhat different in the past compared to the modern ocean. A reorganisation of the marine carbon cycle and its impact on atmospheric CO_2 is not considered here as the available version of HILDA is not set up for such an investigation. Sea surface temperature, affecting CO_2 solubility, and transport parameters were kept constant in all simulations.

2.2 Climate models and climate simulations

ECBILT-CLIO: The global coupled atmosphere-ocean-sea ice model ECBILT-CLIO (version 3.0) includes realistic topography, bathymetry, a simple land surface representation and a bucket water runoff scheme. The atmosphere is represented by the T21, 3-level quasi-geostrophic model ECBILT2 (Opsteegh et al., 1998), which contains a hydrological cycle with clouds prescribed according to the observed zonal mean climatology, and explicitly calculates synoptic variability associated with weather patterns. The ocean model CLIO (Goosse and Fichefet, 1999) is a free-surface ocean general circulation model with a resolution of 3° × 3° and 20 unevenly spaced depth levels, coupled to a thermodynamic-dynamic sea ice model. Temperature and precipitation anomalies as calculated with ECBILT-CLIO were interpolated from the $5.625° \times 5.625°$ resolution of ECBILT2 to the 3.75° longitudinal by 2.5° latitudinal grid used here for the LPJ-DGVM.

Results from a control run (ECBILT-ctrl) and two freshwater discharge experiments ($F_\square$, $F_\triangle$) into the North Atlantic were used (Knutti et al., 2004). These are described in subsection 3.1. The two freshwater experiments differ in the shape and amplitude of the freshwater discharge over time (Fig. 2A). In scenario $F_\triangle$ the discharge strength increases linearly with time to 0.5 Sv (1 Sv = 10^6 m^3 s^{-1}) at $t = t_0 + 500$ yr, then decreases again to zero at $t = t_0 + 1000$ yr, whereas in scenario $F_\square$ the amplitude of the freshwater flux rises instantaneously to 0.3 Sv at t_0 and back to zero 1000 yr later. ECBILT-CLIO simulations were carried out with glacial boundary conditions.

HadSM3: In the sensitivity experiments presented in subsections 3.4 and 3.5, millennial-scale changes in temperature, precipitation, and cloud cover for the last 21 kyr were derived from time slice simulations with the Hadley Centre model HadSM3 (Pope et al., 2000; Hewitt et al., 2001, 2003, Fig. 3C,D). The HadSM3 consists of the HadAM3 atmospheric circulation model (Pope et al., 2000) coupled to a slab ocean model and a sea-ice model as described in Hewitt et al. (2001). The atmosphere has a resolution of 3.75° × 2.5°, with 19 vertical layers.

The climate fields used here are derived from 19 time slices carried out roughly every 1000 years up to preindustrial times. In each time slice, the model is driven by orbital forcing and reconstructed atmospheric CO_2 and methane concentrations. Ice-sheet distribution and sea-level is prescribed according to Peltier (1994) until 7 kyr BP and the present distribution used thereafter. The ocean heat flux convergence in all simulations was held at the same values as derived for present-day conditions. The use of the same heat flux convergence fields is not expected to be of importance for the carbon cycle sensitivity experiments and the findings presented here. The land surface conditions within HadSM3 were varied, by coupling it asynchronously with the BIOME4 equilibrium vegetation model (Kaplan et al., 2002).

2.3 Climate input fields and boundary conditions to force the LPJ-DGVM

Preindustrial freshwater simulations: Climate input fields for the LPJ-DGVM (preindustrial simulations, subsection 3.3) were derived by combining a present-day climatology and the climate anomalies from freshwater experiments obtained with the ECBILT-CLIO model (Knutti et al., 2004). This approach ensures that the LPJ-DGVM is spun-up with observed climate fields and that simulated vegetation distribution at the start of the perturbation experiment is realistic. We did not apply the output fields from the ECBILT-CLIO model directly as ECBILT-CLIO results show a warm bias in the northern mid and high latitudes compared to observations (Timmermann et al., 2004).

The monthly fields for temperature, precipitation, and cloud cover were obtained by adding the updated monthly climatology from Leemans and Cramer (1991) as used in Cramer et al. (2001) together with detrended inter-annual anomalies from observational data (New et al., 2000), and the anomalies (temperature and precipitation) from the ECBILT-CLIO experiments. A 50-year long sequence of the inter-annual variability data was used repetitively. ECBILT-CLIO anomalies were calculated for the two ECBILT-CLIO freshwater experiments and the control run. Absolute monthly mean surface temperature anomalies and relative monthly mean precipitation anomalies with respect to average monthly means of the first 400 years of the ECBILT control experiment (no freshwater forcing) were used. The monthly series for each grid cell were splined using a 50 yr cut-off frequency to remove high-frequency variability already included in the observation-based data.

Sensitivity experiments for different initial climate conditions: Initial climate conditions were varied by adding anomalies from the different HadSM3 time slice simulations to the temperature, precipitation, and cloud cover fields used in the preindustrial experiments. For each time slice, the HadSM3 monthly data were averaged over time and absolute temperature, precipitation, and cloud cover anomalies with respect to the preindustrial monthly means were calculated. Insolation intensity was calculated from orbital parameters (Berger, 1978) and monthly mean cloud cover given by observations and HadSM3 simulation results. Land ice sheet distributions and sea level changes (Fig. 3B) to calculate available land in the LPJ-DGVM were prescribed according to Peltier (1994). This alters the area available for vegetation growth. The net effect is an increase of the area available for vegetation by 7.7 × 10^{12} m^2 from the LGM to modern conditions. Atmospheric CO_2 values used to initialise the

carbon cycle model were taken from ice core data (Monnin et al., 2001) synchronised via CH_4 to the GISP2 age scale (Fig. 3A, Köhler et al., 2005).

2.4 Carbon cycle model spin-up and simulations

Experimental setup: The LPJ-DGVM was spun-up from bare ground for preindustrial conditions and for particular times during the past 21 kyr (6 kyr BP and for each millenia between 11 and 21 kyr BP) by prescribing the corresponding atmospheric CO_2 value and the climate boundary conditions described above. First, the LPJ-DGVM was forced with the observation-based data (Leemans and Cramer, 1991; New et al., 2000) and with the HadSM3 anomalies. At spin-up year 1900, carbon storage of the long-lived soil carbon pools was analytically calculated for each grid cell from input fluxes; then spin-up was continued for another 100 years.

Then, the HILDA ocean model was coupled to the LPJ-DGVM to calculate changes in atmospheric CO_2 and $\delta^{13}C$. For simulation years 2001 to 2400 (years 1 to 400 if the LPJ-DGVM spin-up is neglected in time counting), the anomalies of the last 400 years of the ECBILT control experiment again with respect to average monthly mean values of the first 400 yr of the ECBILT control run were added to the temperature and precipitation fields. The anomalies from the freshwater discharge experiments (either $F_{\square}$ or $F_{\triangle}$) were added for the next 2000 years. Finally, the simulation was continued for another 600 to 2600 years by applying the same forcing as during spin-up. Thus, a simulation run of either 5000 or 7000 yr consists of 2000 yr of spin-up, 2400 yr of experiment, and 600 or 2600 yr of re-equilibration time. Ice sheet extent, sea level, insolation, and the HadSM3 climate anomaly fields were kept constant during each simulation.

Experiments with and without CO_2 fertilisation feedbacks: An increase in atmospheric CO_2 leads to an increase in simulated gross primary productivity, water use efficiency, and carbon storage, similar as in other DGVMs (Cramer et al., 2001). CO_2 fertilisation acts as a negative feedbacks on atmospheric CO_2 perturbations. The magnitude of the CO_2 fertilisation feedbacks in the LPJ-DGVM (e.g. Joos et al., 2001; Sitch et al., 2003; Gerber et al., 2004) is consistent with the enhancement of net primary production shown in free air CO_2 enrichment experiments (DeLucia et al., 1999) and the recent amplification of the seasonal cycle in atmospheric CO_2 (McGuire et al., 2001; Dargaville et al., 2002). There is a debate to which extent CO_2 fertilisation is operating today and in the future to sequester anthropogenic carbon, as co-limitation by other nutrients (e.g. nitrogen) may become important (Hungate et al., 2003). However, a role for CO_2 fertilisation in determining terrestrial carbon storage at CO_2 concentrations within the glacial-interglacial range (190 to 280 ppmv) is generally more accepted and has support from a range of data-based studies (Amthor, 1995; Körner, 2000; Cowling and Field, 2003).

In experiments 'with CO_2 fertilisation feedbacks', atmospheric CO_2 variations calculated from changes in terrestrial storage and the oceanic response were passed to the photosynthesis routine of the LPJ-DGVM. In experiments 'without CO_2 fertilisation feedbacks', the CO_2 value passed to the photosynthesis routine of the LPJ-DGVM was kept constant at its initial value (e.g. 190 ppmv for LGM condition; 280 ppmv for preindustrial condition) throughout the experiment. Thus, the modelled CO_2 changes do not affect the modelled changes in the terrestrial system.

Simulated changes in terrestrial carbon storage and atmospheric CO_2 and $\delta^{13}C$ are substantially smaller in simulations with CO_2 fertilisation feedbacks than without. In the following figures, we mainly show results from simulations without CO_2 fertilisation feedbacks for the following reasons. The ratio of the response of the terrestrial biosphere to the collapse of the NA THC (signal) to variations caused by high frequency climate variability (noise) is higher in the experiments without fertilisation. This makes interpretation of the results easier as the difference between the NA THC induced response and the control run variability becomes larger. Results of experiments without CO_2 fertilisation feedbacks are independent from a potential contribution of the marine carbon cycle to atmospheric CO_2 variations. In experiments which consider CO_2 fertilisation feedbacks such a marine contribution would further modify the land carbon storage anomalies and are thus not independent from a potential coupling of the terrestrial and marine parts of the carbon cycle. Neglecting CO_2 fertilisation provides an upper limit to the changes in terrestrial carbon storage within the experimental setup of this study.

3 Results

3.1 ECBILT-CLIO climate model results for freshwater discharge experiments

The freshwater discharge experiments performed with ECBILT-CLIO lead to the typical climate anomalies of the bipolar seesaw. Both experiments ($F_{\square}$, $F_{\triangle}$) result in a collapse of the North Atlantic Deep Water formation (NADW export at 30°S drops from 17 to 3 Sv, Fig. 2B), a drop in North Atlantic near surface air temperature by about 10 K and a warming of the Southern Ocean near surface air by approximately 4 K (Fig. 2C, for details see Knutti et al., 2004). While in $F_{\square}$ the magnitude of the NADW formation drops below 5 Sv about 100 yr after the start of the freshwater discharge, it takes nearly 400 yr for the shut-down of the deep water formation in the $F_{\triangle}$ experiment. The NADW formation starts to recover immediately at the end of the freshwater discharge and is back to full strength after 300 yr in scenario $F_{\triangle}$, while this recovery process is delayed by a further 200 yr in scenario $F_{\square}$ (Fig. 2B,C). Temperature anomalies are closely coupled to NADW formation and thus the cooling in the north is prolonged by the same 200 yr in the $F_{\square}$ experiment relative to $F_{\triangle}$.

Temperature perturbations over land are mainly restricted to northern mid and high latitudes (Fig. 4), the zonally-averaged temperature drops over ice-free land by as much

as 7 K at $70-80°$N. The induced warming in the Southern Ocean impacts the southernmost tip of South America only. Precipitation patterns are perturbed worldwide (Fig. 4) leading to a reduction in rain fall over parts of Central Asia, the Mediterranean region, Northern Africa, and near the equator in South America, whereas rain fall increases south of $10°$S (Southern South America, Southern Africa, Australia), and Eastern Asia and North America.

The choice of the initial climatic boundary conditions applied in ECBILT-CLIO is of little importance for this study. The ECBILT-CLIO model yields very similar changes in temperature and precipitation over land in response to a freshwater discharge and a NA THC collapse under glacial and interglacial boundary conditions (supplementary information in Knutti et al., 2004). Differences in the overturning are small between simulations with preindustrial and Last Glacial Maximum boundary conditions (Timmermann et al., 2004). The convective area in the NA is only slightly shifted southwards for the ECBILT-CLIO LGM simulation compared to the experiment with preindustrial boundary conditions. It has been shown that deep-water formation in ocean models depends strongly on a number of parameters and processes, e.g. on wind stress (Timmermann and Goosse, 2004), on the freshwater budget (Gent, 2001) and on ocean mixing parameterisations (Knutti et al., 2000). Here, no attempt was made to tune the CLIO model towards a specific behaviour.

3.2 Carbon and vegetation distribution for LGM and preindustrial conditions

The simulated transient millennial-scale evolution of terrestrial carbon storage and vegetation distribution over the past 21 kyr has been described elsewhere (Kaplan et al., 2002; Joos et al., 2004). Both studies suggest that global terrestrial carbon storage increased during the transition and the early Holocene and remained relatively stable until the onset of the industrialisation. We expect that the terrestrial response to a NA THC collapse depends on the initial conditions.

The simulated potential natural vegetation for preindustrial time (here and in the following taken at 1 kyr BP) shows the main features indicated in observation-based maps and in other DGVMs (e.g. Haxeltine and Prentice, 1996; Cramer et al., 2001). The maximum carbon storage per unit area is found in the boreal forests of the northern high latitudes ($40-70°$N) with peak values around 70 kg m^{-2} (Fig. 5 top). Here, at least 60% of the carbon is stored in the soil pools, while in the tropical forests two thirds and more of the carbon is generally allocated in the living vegetation.

The simulated biome distribution for the LGM differs radically from the present-day distribution, which is also mirrored in the total carbon content per unit area (Fig. 5 middle), and reproduces the broad features observed in paleodata. Strong reduction in temperatures in northern latitudes produces a southward displacement and major reduction in area of the boreal forest, while reduced precipitation over mid-latitude Eurasia causes a fragmentation of the temperate forests. These features are consistent with observations, as summarised e.g. in Prentice et al. (2000). However, despite the reduced precipitation, the simulations show forest over much of western Europe whereas the data show even drier conditions with steppe predominant. The reconstructions also show a reduced extent of tropical forests and increased extent of grasslands and shrub-lands. Carbon storage in high northern latitude is largely reduced (Fig. 5 bottom). The maximum carbon storage per unit area is further south than at 1 kyr BP. Additional land area available for vegetation due to the sea level drop by about 120 m is mainly found in the Indo-Malaysian archipelago and the Bering Strait. The total carbon storage at 1 kyr (21 kyr) BP is 2919 (2142) PgC, consisting of 922 (629), 471 (299), and 1525 (1214) PgC stored in vegetation, litter, and soil, respectively. In summary, less carbon is available for a potential release in response to a climatic perturbation at the LGM than at preindustrial times.

The total modelled terrestrial carbon inventory of 2900 PgC is comparable to the recent estimate of 3000 PgC (excluding soil carbon stored in wetlands and frozen soils; Sabine et al., 2004). The simulated increase of 780 GtC in terrestrial carbon stock since glacial times is slightly higher than the range of 300 to 700 PgC inferred from marine δ^{13}C sediment data and at the lower end of estimates based on pollen data (range 700 to 1400 PgC) (see Joos et al. (2004) for references).

3.3 Carbon cycle model simulations for preindustrial initial conditions

This subsection presents results of simulations for the preindustrial background state and with and without CO_2 fertilisation feedbacks. Changes in vegetation distribution, global terrestrial carbon storage, and atmospheric CO_2 and δ^{13}C in response to a NA THC collapse are described first, before the governing mechanisms and spatio-temporal changes are discussed in more detail.

The cooling in northern latitudes causes a southward movement of the treeline and a decrease in forested area (Figs. 6, 7). Boreal trees are replaced by grasses north of $50°$N. The reduction in tree coverage leads to a loss of carbon storage in vegetation in northern high latitudes. Temperate trees are partly replaced by grasses and boreal trees between $30-60°$N (Fig. 6). On the other hand, tree coverage is increased in parts of Eastern Asia around $40°$N (Fig. 7). These changes in vegetation distribution are largely independent of the CO_2 fertilisation feedback mechanism.

The global carbon inventory varies by about 40 (70) PgC for the simulation with (without) CO_2 fertilisation feedbacks (Fig. 8). Peak-to-peak difference in carbon storage is 70 (120) PgC. The response of global terrestrial carbon storage to the climatic perturbations shows a complex temporal evolution. The initial response to the THC slowing and NH cooling is a terrestrial uptake of 30 (50) PgC (Fig. 8). Then, the same amount is released during the collapsed state of the THC starting approximately a century after THC reached its minimum. A further release of 40 (70) PgC occurs during the

THC recovery and NH warming after the end of the freshwater discharge. Finally, an uptake of similar amounts occurs during the equilibration phase after the end of the warming.

Atmospheric CO_2 varies by 13 (22) ppmv (peak-to-peak) in the simulation with (without) CO_2 fertilisation feedbacks (Fig. 9). CO_2 first drops by 5 ppmv and then increases to a concentration that is 8 ppmv higher than before the freshwater release in the standard experiment with fertilisation feedbacks. The increase in the atmospheric carbon inventory corresponds to about a third to half of the decrease in the terrestrial inventory (1 ppmv = 2.123 PgC). In other words, about half to two thirds of the cumulative terrestrial release and uptake is buffered by oceanic carbon uptake and release. The atmospheric variations are dampened if the model's CO_2 fertilisation feedback mechanism is operating. A substantial part of the atmospheric perturbation is then mitigated through uptake and release stimulated by the physiological effects of CO_2 on plants.

Atmospheric δ^{13}C fluctuates by 0.25 (0.40) ‰ in the simulation with (without) CO_2 fertilisation feedbacks (Fig. 9). δ^{13}C varies in opposite direction to atmospheric CO_2. Through photosynthesis terrestrial carbon is depleted in its heavy stable isotope content with respect to the atmosphere. Carbon uptake (release) by the land biosphere causes atmospheric CO_2 to decrease (increase) and δ^{13}C to increase (decrease). The atmospheric δ^{13}C perturbation is mitigated by exchange with the ocean and the land biosphere.

In summary, the climate fluctuations associated with a (hypothetical) NA THC collapse and recovery for preindustrial conditions cause atmospheric CO_2 to vary by 10 to 20 ppmv within about 1000 years. Results are similar for the rectangular and triangular freshwater experiments (Fig. 10A). Uptake and release are 200 yr earlier in experiment $F_\Box$ than in $F_\triangle$.

Next, the underlying mechanisms and processes are investigated. Two factorial experiments were performed where either only the temperature or only the precipitation anomalies from the ECBILT-CLIO control run were used. Changes in temperature are mainly responsible for the modelled global terrestrial stock changes, whereas precipitation changes are of less importance on a global scale (Fig. 10B).

The complex transient evolution of the global carbon stocks (Fig. 11A) can be explained in the context of the regional changes in carbon storage (Fig. 12). Global stocks are affected by regional changes in vegetation distribution, growing conditions, as well as changes in the soil respiration rates. Cooling leads to decreased soil respiration rates and tends to increase carbon storage in the modelled soil pools, whereas warming leads to increased respiration rates and carbon release. Better growing conditions lead to higher production and litter fluxes and to an increase in vegetation and soil carbon.

The spatio-temporal pattern of total carbon shown in Fig. 12 reveals a reduced total carbon storage north of 55°N and an increased carbon storage in northern mid latitudes during the cold phase of the experiment. This pattern is related to a loss of vegetation and soil carbon in response to forest dieback in the north and to increased carbon storage in mid latitudes due to improved growing conditions and reduced soil respiration rates in response to cooling. Changes in globally-integrated vegetation carbon are small. Reduced local storage in vegetation is compensated by increased vegetation storage elsewhere (Fig. 11A). In particular, vegetation carbon is reduced in areas of forest decline and increased due to more favourable growth conditions in the areas south of the retreating forests.

Overturning times of soil carbon stocks vary between the north and mid-latitude regions and this implies a different response time to a climate perturbation. We note that the decrease in total carbon storage in the high north occurs later than the increase in storage in northern mid latitudes (Fig. 12). Similarly, high-latitude carbon storage remains reduced for several centuries after the THC recovery, whereas the mid-latitude anomaly disappears during the THC recovery. Modelled soil overturning is relatively fast in warm and humid tropical regions, modest in temperate regions, but very slow in the cold high latitudes. The gross of the litter and soil pools in mid-latitude reacts within centuries to the THC-induced climatic changes. The relatively fast response of soils in mid-latitude compared to the north is mainly responsible for the initial increase in global carbon storage after the NA THC collapse (simulation year 400 to 700) and the decrease during the THC recovery (year 1400 to 1900). The release and build-up of soil carbon stocks in high northern latitude is a slow process. The high-latitude forests decline in response to cooling leads to net carbon release from vegetation and from soils dominating the global stock changes during the collapsed state (year 700 to 1400). The build-up of the soil pools in high northern latitudes takes many centuries after the NA THC has recovered again.

Precipitation changes (Fig. 4) causes relatively minor changes in global carbon stocks (Fig. 10B). Generally drier conditions between 5°S and 15°N lead to a partial replacement of tropical trees by grasses and a slight decrease in the amount of carbon stored in vegetation followed by a reduction in soil carbon storage. Enhanced precipitation between 10°S and 20°S induces a shift from grassland to tropical forests and soil carbon build up (Fig. 12). Wetter conditions in Eastern Asia at 40°N promote the increase in tree coverage there (Fig. 7). These shifts in vegetation cover are reversed in most grid cells towards the end of the simulation. However, in a few grid cells in tropical South America the change from grasses to rain-green trees is persistent. Once trees have been established, they hinder grass from growing using the available water. This persistent shift in a few grid cells is the reason that carbon storage is higher by 35 PgC at the end than at the start of the experiment. Similar changes, although with different magnitude and in different regions, are found in all simulations.

In conclusion, the global evolution of carbon uptake and release is governed by a subtle combination of different processes operating on different time scales in different regions. This implies that different initial conditions may lead to a very different transient response in global carbon storage and atmospheric CO_2 to a THC collapse and recovery. This is ex-

amined in the next subsection.

3.4 Sensitivity to the initial climate condition

Figure 13 shows global carbon stock changes in response to a THC collapse and recovery for experiments started at different times during the last 21 kyr. The peak-to-peak variations in global terrestrial carbon stock are of order 50 PgC (100 PgC) in the various simulations with (without) CO_2 fertilisation feedbacks. However, the transient evolution of global carbon stock changes varies greatly between the different runs. Global terrestrial carbon inventory increases with the THC collapse and remains high until the THC has recovered in simulations starting during the late phase of the glacial-interglacial transition and the early Holocene. In contrast, global carbon storage is, after a small initial increase, reduced to reach a minimum at the end of the freshwater release in the simulation starting at the LGM. Results are similar as obtained for the preindustrial runs for experiments starting during the first half of the transition (18 to 16 kyr BP) but with smaller amplitudes.

Atmospheric CO_2 is reduced during the phase of a collapsed THC in experiments starting between 15 and 6 kyr BP, but increased for the experiments starting from LGM conditions (Fig. 9 left). The amplitude in the atmospheric CO_2 variations is smaller for experiments starting at conditions (climate, CO_2, land mask) typical for the LGM and early transition than for experiments starting at higher CO_2 levels, reduced land ice sheets, and warmer periods. The atmospheric CO_2 peak around the THC collapse and recovery is only 6 ppmv for LGM conditions and with CO_2 fertilisation feedbacks operating (Fig. 9 left). Similarly, δ^{13}C variations are very small (< 0.2 ‰) in this experiment (Fig. 9 right).

The temporal response of the terrestrial system to a THC collapse is sensitive to the vegetation and soil distribution at the beginning of the experiments. Different distributions imply different relative importance of the governing mechanisms discussed in the previous subsection. In all simulations, respiration rates are reduced in response to cooling, tending to enhance soil carbon storage. This results in an initial increase in terrestrial storage in all simulations. Forest decline in the north and a southward shift of the northern treeline occurs in all simulations (Fig. 7). This is evident in reduced carbon storage in the regions where the treeline has shifted, i.e. around 65°N for preindustrial conditions and 55°N for glacial initial conditions (Fig. 12). However, the area of enhanced growing conditions and increased soil storage around 40°N is largely compressed under the cold glacial conditions as the tree line is generally found further south. Thus, the balance of carbon loss in the north and carbon gain further south is shifted between experiments. For preindustrial and Holocene conditions, the increase in mid-latitude carbon stocks is larger than the reduction in the north during the collapsed state of the THC, whereas the opposite is the case for the experiment with LGM boundary conditions (Fig. 11, 12).

Factorial experiments were performed to further explore the sensitivity of results to initial climate conditions and individual environmental variables. The applied land mask (ice sheet extent and sea level), the climatic fields (temperature, precipitation, and cloud cover), or the initial CO_2 concentration were set individually to their preindustrial ($t = 1$ kyr BP) or glacial ($t = 21$ kyr BP) values. We note that the modelled glacial-interglacial increase in terrestrial inventories of around 780 PgC is predominantly driven by CO_2 fertilisation in response to the increase in atmospheric CO_2 of about 80 ppmv (Joos et al., 2004), whereas changes in climate exert a smaller influence on the modelled glacial-to-preindustrial change in global carbon storage on land (vegetation-climate feedbacks have been neglected in these off-line simulations with the LPJ-DGVM).

The climatic (background) field is the most important one among the input variables land mask, climate, and CO_2 for the simulated variations in terrestrial carbon and atmospheric CO_2 in response to THC changes (Fig. 14 left). The reason is that the climatic fields largely determine the competition between individual plant functional types and thus govern simulated vegetation and soil distribution. In turn, the initial distribution of vegetation and soil carbon has a dominant influence on the transient response to a THC collapse and recovery. The simulated response is similar in all simulations where the LGM fields are applied irrespective of the land mask and atmospheric CO_2 level. Similarly, the transient evolution in carbon storage is comparable in all simulations where the preindustrial climate fields are applied. The increase in atmospheric CO_2 by about 80 ppmv from LGM to preindustrial levels tends to increase the amplitude of the simulated changes as generally much more carbon is stored on land under higher CO_2 in the LPJ-DGVM. Changes in the applied land mask induce small changes in the carbon storage variations for experiments starting at 1 and 13 kyr BP, but have nearly no influence on the transient response in earlier times. In a glacial climate, growing conditions in terms of temperature over the area of the northern hemispheric land ice shields are so unfavourable that no or only very little vegetation establishes in these areas now additionally available for the terrestrial biosphere. The climatic perturbations from the THC changes are too small over the area of the former Laurentide ice sheet to influence results substantially.

In conclusion, the initial vegetation (plant functional type) distribution is very important for the transient response of the terrestrial system to a THC collapse and recovery. Thus, the transient response to a northern hemisphere cooling-warming event is very sensitive to the initial climate conditions. Simulated atmospheric CO_2 and δ^{13}C variations associated with THC changes are of the order of 15 ppmv and 0.3‰, respectively, for preindustrial conditions and about half these amplitudes for LGM conditions.

3.5 Sensitivity to the magnitude of the temperature perturbation

In a further sensitivity study we analyse how the response patterns depend on the magnitude in the temperature fluctuations which were identified as the dominant variables determining the carbon storage anomalies for a NA THC shutdown (Fig. 14 right). We vary the monthly ECBILT-CLIO temperature anomalies in each grid cell by $+25\%$, -25%, or -50%. The variations by $\pm 25\%$ induce only small changes in carbon storage for initial conditions corresponding to 1 and 13 kyr BP. At 17 and 21 kyr BP an increase in the temperature anomalies increases the carbon release in the cold phase by $\sim$50 PgC. A reduction in temperature anomalies by 50% reduces the amplitudes in the carbon storage anomalies at all times and also leads to a remarkable reduction in the soil carbon gain by a smaller decrease in soil respiration during the initial northern hemispheric cooling. These sensitivity experiments result in well distinguishable responses especially for LGM boundary conditions.

4 Discussion and Conclusion

Experiments on the transient terrestrial response to a temporary northern hemispheric cooling induced by a collapse of the North Atlantic thermohaline circulation (THC) have been performed using the Lund-Potsdam-Jena Dynamic Global Vegetation Model (LPJ-DGVM) in an idealised setting. Changes in atmospheric CO_2 caused by a reorganisation of the marine carbon cycle have not been addressed. However, ocean uptake of carbon released from the terrestrial biosphere has been taken into account. The experimental setup is complementary to and mirrors that of earlier ocean modelling studies that investigated changes in the marine carbon cycle and their impact on CO_2, but neglected changes on land (Marchal et al., 1998; Ewen et al., 2004). The perturbation experiments were run with different climate, CO_2, and ice sheet initial boundary conditions spanning the range from the Last Glacial Maximum to preindustrial times. The sensitivity of the results to individual forcing factors (temperature, precipitation, ice sheet extent, CO_2) and with respect to CO_2 fertilisation feedbacks acting in the LPJ-DGVM were investigated.

The main results of this study are as follows. The northern hemisphere cooling after a THC collapse leads to a southward movement of the treeline and a reduction in the extent of boreal and temperate forests. Changes in global terrestrial carbon storage and implied changes in atmospheric CO_2 and $\delta^{13}C$ are small. CO_2 fertilisation feedbacks operating in the LPJ-DGVM and exchange with the ocean dampen the impact of terrestrial carbon uptake and release on atmospheric CO_2. The modelled terrestrial response to a THC collapse depends sensitively on the climatic initial condition and the associated spatial distribution of vegetation and carbon on land. For glacial conditions, modelled atmospheric CO_2 varies only by 6 ppmv due to terrestrial changes in response to the THC collapse compared to a 13 ppmv peak-to-peak variation under preindustrial climate conditions.

An important result of our study is that not only the magnitude of the peak-to-peak CO_2 variations, but also the specific temporal evolution of carbon uptake and release depends strongly on the initial climate condition and vegetation distribution. For example, the terrestrial carbon inventory is reduced during the cold phase and during the following few centuries for the run with glacial boundary conditions, whereas storage is increased during the entire cold phase for the run with boundary conditions for 13 kyr BP. This emphasises the importance of the general climatic setting for the terrestrial response to a THC collapse. The impact of the same climatic perturbation on atmospheric CO_2 can be of opposite sign depending on the initial condition and climatic background (Fig. 9).

There are a number of limitations that could affect the results. The LPJ-DGVM was forced with prescribed climate fields. Hence, changes in vegetation cover and associated changes in surface albedo, roughness and evapotranspiration simulated by the LPJ-DGVM do not feed back to the atmosphere. These feedbacks could amplify the climatic changes simulated by the climate model. For example, increased surface albedo due to a dieback of trees in high latitudes could lead to additional cooling and reduction of tree coverage.

The dynamics of wetlands and peats are not explicitly modelled in the LPJ-DGVM. However, we do not expect that the net carbon fluxes between wetlands and peats and the atmosphere are changed significantly after a collapse of the NA THC as the associated cooling over Eurasia will probably slow both carbon accumulation as well as carbon loss from these systems.

The quasi-geostrophic atmosphere of the ECBILT-CLIO model represents tropical dynamics only incompletely. Simulated changes in precipitation around the equator and implied changes in tropical carbon storage must therefore be considered with caution. Precipitation changes cause a persistent replacement of grass by rain-green trees in a few subtropical grid cells and in all simulations. The new vegetation cover remains stable after NA THC has recovered and the climate perturbation has disappeared. This results in higher carbon storage at the end compared to the start of an experiment. This increase amounts to 35 PgC in the preindustrial standard experiment $F_{\square}$, compared to a simulated peak-to-peak difference of 120 PgC.

Changes in atmospheric CO_2 caused by a reorganisation of the marine carbon cycle affect terrestrial storage through the CO_2 fertilisation mechanism. In this study, the contribution of changes in the marine carbon cycle to terrestrial carbon stock changes through CO_2 fertilisation has not been considered. It is likely that this link between the marine and terrestrial system had a large influence on the total terrestrial carbon stock changes during past climatic perturbations.

The principle response of the vegetation to the cooling, a decrease in the extent of boreal and temperate trees, reflects main findings from pollen records (Peteet, 1995). A direct comparsion of our results with Peteet (1995), how-

ever, is difficult as the NA THC was probably not entirely stopped during the YD. The vegetation changes are similar to those simulated by Scholze et al. (2003b) and we refer to their work for a more detailed discussion and a comparison between modelled and reconstructed vegetation changes.

The comparison of our results with the work of Scholze (2003) and Scholze et al. (2003b) seems to confirm the finding of this study that the terrestrial response depends sensitively on initial climate conditions and vegetation distribution. These authors simulated larger changes and a different evolution of the terrestrial carbon stock and atmospheric CO_2 in response to a THC collapse than simulated here for a comparable experiment (preindustrial initial conditions, no CO_2 fertilisation feedbacks in the LPJ-DGVM). Scholze and co-workers forced the same model as used here, the LPJ-DGVM, but with output from a different climate model, the ECHAM3/LSG. The climatic perturbations after a THC collapse simulated by ECHAM3/LSG are similar in its spatial pattern but smaller in amplitude than those simulated by ECBILT-CLIO (e.g. a cooling of 4 K over larger parts of northern Eurasia in ECHAM3/LSG versus 6–8 K in ECBILT-CLIO). Thus, the difference in the response of the two models to a NA THC collapse can not explain the larger response found by Scholze et al. (2003b). We suggest that the differences between results by Scholze et al. (2003b) and our study may be caused by the difference in the applied initial climate conditions.

The ice core CO_2 record (Indermühle et al., 2000; Monnin et al., 2001) provides an important observational constraint on simulated changes in atmospheric CO_2 in response to a NA THC collapse. However, reconstructed atmospheric CO_2 reflects all changes in the marine and terrestrial carbon cycle, whereas the reorganisation of the marine carbon cycle and changes that are not directly related to changes in the NA THC are not captured in our model setup.

For the period from 60 to 20 kyr BP, Indermühle et al. (2000) found multi-millennial CO_2 variations of around 20 ppmv that parallel the Antarctic warm events A1 to A4 which are associated with the Heinrich events 4, 5, 5a, and 6 (Fig. 1). The ice core CO_2 record has a limited temporal resolution through the limited number of samples and the broad age distribution of air enclosed in the bubbles of the ice (Indermühle et al., 2000; Monnin et al., 2001). Seventy-three data points are available for the period from 60 to 20 kyr BP, i.e. on average one point every 550 years. The simulated peak-to-peak CO_2 variations for a complete THC collapse and recovery are less than 13 ppmv within a period of less than 2000 year in the runs with CO_2 fertilisation feedbacks for any of the applied initial conditions and less than 6 ppmv for typical glacial conditions (21 and 17 kyr BP simulation). The model results for atmospheric CO_2 are well within the range of variations and the rate of change found in the ice core record (Indermühle et al., 2000) for the Antarctic warm events.

Results from ocean modelling and observation-based studies provide information on how changes in the marine carbon cycle might have affected atmospheric CO_2 during a NA THC slow down. Simulations with dynamic ocean models (Marchal et al., 1998; Ewen et al., 2004) suggest that atmospheric CO_2 increased after a THC collapse by 10 to 15 ppmv in response to marine changes only. However, the causes for the simulated rise in CO_2 are different, as Ewen et al. (2004) used an abiotic ocean model, whereas Marchal et al. (1998) applied a model that represents both physico-chemical and biological processes. High resolution Antarctic dust records (Röthlisberger et al., 2004) suggest that a decrease in aeolian iron input into the Southern Ocean might via iron limitation of the marine export production have contributed up to 20 ppmv to the reconstructed CO_2 increase during the warm periods of the Antarctic A1 to A4 events. In summary, the available evidence suggests that changes in the marine carbon cycle contributed to the rise in atmospheric CO_2 for each of the A1 to A4 events. Consequently, the contribution of terrestrial changes to the CO_2 increase must have been smaller than found in the ice core record. We conclude that the results of this study are compatible with the ice core record and the available studies of the marine carbon cycle.

CO_2 variations were less than a few ppmv during climate perturbations others than the Antarctic warm/Heinrich events, when the NA THC was probably only partly collapsed (Indermühle et al., 2000). No detectable CO_2 variations are found in the ice core data around the 8.2 kyr BP northern hemispheric cold event (Monnin et al., 2004). Similarly, very small changes in atmospheric CO_2 are simulated in sensitivity experiments in which the ECBILT-CLIO temperature anomalies were reduced by 50% to mimic the effect of a partial NA THC collapse.

For the glacial-interglacial transition, the situation is complex and many different processes affected atmospheric CO_2. Monnin et al. (2001) found rates of increase in atmospheric CO_2 of 20 ppmv per kyr during the YD period (13.0 to 12.8 kyr BP, all ages given here on the GISP2 age scale) and during 18.0 to 16.5 kyr BP and slower growth rates in between including the Bølling-Allerød. Work by McManus et al. (2004) and Skinner and Shackleton (2004) suggests that the NA THC was reduced during the YD period and the Heinrich 1 iceberg discharge event and was operating at a near interglacial mode during the Bølling-Allerød warm phase. Again, the magnitude of the simulated atmospheric CO_2 variations around a collapse and an onset of the THC is compatible with the reconstructed CO_2 evolution during the transition when taking into account that other ocean-related carbon cycle changes were occurring as well (Broecker and Henderson, 1998; Köhler et al., 2005).

An interesting feature of the CO_2 record are two step-like increases by 6 and 8 ppmv at the end of the YD cold period and at the onset of the Bølling-Allerød warm period (Monnin et al., 2001), when the THC recovered from a largely reduced or collapsed state. These step-like changes occur within the temporal resolution of the data, i.e. within two to three centuries. A rapid increase by a few ppmv in less than a few decades is found together with the resumption of the THC in the simulations starting during the transition (e.g. 13 kyr simulation in Fig. 9). It is tempting to speculate that the observed

step-like increases of 6 to 8 ppmv at times when the NA THC resumed were, at least partly, caused by associated changes in terrestrial carbon storage. However, the subsequent drop in CO_2 found in the simulation is not evident in the data.

Simulated changes in atmospheric δ^{13}C in response to the terrestrial changes are about 0.2 ‰ for glacial boundary conditions. This suggests that terrestrial carbon changes in response to a THC collapse partly contributed to the reconstructed glacial δ^{13}C variations of the order of 0.3 ‰ during Heinrich event 1 or the YD cold event (Smith et al., 1999).

In conclusion, simulated changes in terrestrial carbon inventories and atmospheric CO_2 in response to changes in the NA THC are compatible with the available ice core CO_2 record over the glacial period, the last transition, and the early Holocene and the available marine studies. The modelled response in terrestrial carbon storage is sensitive to the initial climatic conditions, vegetation distribution and the magnitude of the CO_2 fertilisation feedback mechanism.

Acknowledgements. We thank Paul Valdes for providing output from his time slice simulations with the Hadley Centre model. Comments by Kuno Strassmann and the reviews of Michel Crucifi x and two anonymous reviewers are appreciated. This study was performed during a three months visit of PK at the Department of Climate and Environmental Physics of the University of Bern. Funding by the Swiss National Science Foundation and by the German Ministry of Education and Research (BMBF) through the German climate research program DEKLIM (project RESPIC) is acknowledged.

References

Amthor JS (1995) Terrestrial higher-plant response to increasing atmospheric [CO_2] in relation to the global carbon cycle. Global Change Biology 1: 243–274

Berger AL (1978) Long-term variations of daily insolation and Quaternary climatic changes. Journal of Atmospheric Sciences 35: 2362–2367

Blunier T, Brook EJ (2001) Timing of millennial-scale climate change in Antarctica and Greenland during the last glacial period. Science 291: 109–112

Blunier T, Chappellaz J, Schwander J, Dällenbach A, Stauffer B, Stocker TF, Raynaud D, Jouzel J, Clausen HB, Hammer CU, Johnsen SJ (1998) Asynchrony of Antarctic and Greenland climate change during the last glacial period. Nature 394: 739–743

Blunier T, Schwander J, Chappellaz J, Parrenin F, Barnola JM (2004) What was the surface temperature in central Antarctica during the Last Glacial Maximum? Earth and Planetary Science Letters 218: 379–388

Bond G, Broecker W, Johnsen S, McManus J, Labeyrie L, Jouzel J, Bonani G (1993) Correlations between climate records from North Atlantic sediments and Greenland ice. Nature 365: 143–147

Bond GC, Lotti R (1995) Iceberg discharges into the North Atlantic on millennial time scales during the last glaciation. Science 267: 1005–1010

Broecker WS (1998) Paleocean circulation during the last glaciation: A bipolar seesaw? Paleoceanography 13(2): 119–121

Broecker WS, Henderson GM (1998) The sequence of events surrounding Termination II and their implications for the cause of glacial-interglacial CO_2 changes. Paleoceanography 13(4): 352–364

Brook EJ, Harder S, Serveringhaus J, Steig EJ, Sucher CM (2000) On the origin and timing of rapid changes in atmospheric methane during the last glacial period. Global Biogeochemical Cycles 14: 559–572

Brook EJ, Sowers T, Orchardo J (1996) Rapid variations in atmospheric methane concentration during the past 110,000 years. Science 273: 1087–1091

Collatz GJ, Ribas-Carbo M, Berry JA (1992) A coupled photosynthesis – stomatal conductance model for leaves of C_4 plants. Australian Journal of Plant Physiology 19: 519–538

Cowling SA, Field CB (2003) Environmental control of leaf area production: Implications for vegetation and land-surface modeling. Global Biogeochemical Cycles 17: 1007, doi: 10.1029/2002GB001915

Cramer W, Bondeau A, Woodward FI, Prentice IC, Betts RA, Brovkin V, Cox PM, Fisher V, Foley JA, Friend AD, Kucharik C, Lomas MR, Ramankutty N, Sitch S, Smith B, White A, Young-Molling C (2001) Global response of terrestrial ecosystem structure and function to CO_2 and climate change: results from six dynamic global vegetation models. Global Change Biology 7: 357–375

Crowley TJ (1992) North Atlantic deep water cools the southern hemisphere. Paleoceanography 7: 489–497

Dansgaard W, Clausen HB, Gundestrup N, Hammer CU, Johnsen SF, Kristinsdottir PM, Reeh N (1982) A new Greenland deep ice core. Science 218: 1273–1277

Dargaville RJ, Heimann M, McGuire AD, Prentice IC, C. I, Kicklighter DW, Joos F, Clein JS, Esser G, Foley J, Kaplan J, Meier RA, Melillo JM, Moore B, Ramankutty N, Reichenau T, Schloss A, Sitch S, Tian H, Williams L, Wittenberg U (2002) Evaluation of terrestrial carbon cycle models with atmospheric CO_2 measurements: Results from transient simulations considering increasing CO_2, climate, and land-use effects. Global Biogeochemical Cycles 16: 1092, doi: 10.1029/2001GB001426

DeLucia EH, Hamilton JG, Naidu SL, Thomas RB, Andrews JA, Finzi A, Lavine M, Matamala R, Mohan JE, Hendrey GR, Schlesinger WH (1999) Net primary production of a forest ecosystem with experimental CO_2 enrichment. Science 284: 1177–1179

Ewen TL, Weaver AJ, Schmittner A (2004) Modelling carbon cycle feedbacks during abrupt climate change. Quaternary Science Reviews 23: 431–448

Farquhar GD, von Caemmerer S, Berry JA (1980) A biochemical model of photosynthetic CO_2 assimilation in leaves of C_3 species. Planta 149: 78–90

Foley J (1995) An equilibrium model of the terrestrial carbon budget. Tellus 47B: 310–319

Gent (2001) Will the North Atlantic Ocean thermohaline circulation weaken during the 21st century? Geophysical Research Letters 28: 1023–1026

Gerber S, Joos F, Brügger P, Stocker TF, Mann ME, Sitch S, Scholze M (2003) Constraining temperature variations over the last millennium by comparing simulated and observed atmospheric CO_2. Climate Dynamics 20: 281–299

Gerber S, Joos F, Prentice IC (2004) Sensitivity of a dynamic global vegetation model to climate and atmospheric CO_2. Global Change Biology 10: 1223–1239, doi: 10.1111/j.1365–2486.2004.00807.x

Goosse H, Fichefet T (1999) Importance of ice-ocean interactions for the global ocean circulation: A model study. Journal of Geo-

physical Research 104: 23337–23355
Grootes PM, Stuiver M (1997) Oxygen 18/16 variability in Greenland snow and ice with 10^3 to 10^5-year time resolution. Journal of Geophysical Research 102: 26455–26470
Haxeltine A, Prentice IC (1996) BIOME3: An equilibrium terrestrial biosphere model based on ecophysiological constraints, resource availability, and competition among plant functional types. Global Biogeochemical Cycles 10: 693–709
Heinrich H (1988) Origin and consequences of cyclic ice rafting in the northeast Atlantic ocean during the past 130,000 years. Quaternary Research 29: 142–152
Hemming SR (2004) Heinrich events: massive late Pleistocene detritus layers of the North Atlantic and their global climate imprint. Reviews of Geophysics 42: RG1005, doi: 10.1029/2003RG000128
Hewitt CD, Senior CA, Mitchell JFB (2001) The impact of dynamics sea-ice on the climatology and climate sensitivity of a GCM: A study of past, present, and future climates. Climate Dynamics 17: 655–668
Hewitt CD, Stouffer RJ, .Broccoli AJ, Mitchell JFB, Valdes PJ (2003) The effect of ocean dynamics in a coupled GCM simulation of the Last Glacial Maximum. Climate Dynamics 20: 203–218
Hungate BA, Dukes JS, Shaw MR, Luo Y, Field CB (2003) Nitrogen and climate change. Science 302: 1512–1513
Indermühle A, Monnin E, Stauffer B, Stocker TF (2000) Atmospheric CO_2 concentration from 60 to 20 kyr BP from the Taylor Dome ice core, Antarctica. Geophysical Research Letters 27: 735–738
Johnsen SJ, Clausen HB, Dansgaard W, Fuhrer K, Gundestrup N, Hammer CU, Iversen P, Jouzel J, Stauffer B, Steffensen JP (1992) Irregular glacial interstadials recoreded in a new Greenland ice core. Nature 359: 311–313
Johnsen SJ, Dahl-Jensen D, Dansgaard W, Gundestrup N (1995) Greenland palaeotemperatures derived from GRIP bore hole temperature and ice core isotope profi les. Tellus 47B: 624–629
Johnsen SJ, Dansgaard W, Clausen HB, Langway-Jr CC (1972) Oxygen isotope profi les through the Antarctic and Greenland ice sheets. Nature 235: 429–434
Joos F, Bruno M, Fink R, Siegenthaler U, Stocker TF (1996) An effi cient and accurate representation of complex oceanic and biospheric models of anthropogenic carbon uptake. Tellus 48B(3): 397–417
Joos F, Gerber S, Prentice IC, Otto-Bliesner BL, Valdes PJ (2004) Transient simulations of Holocenic atmospheric carbon dioxide and terrestrial carbon since the Last Glacial Maximum. Global Biogeochemical Cycles 18: GB2002, doi: 10.1029/2003GB002156
Joos F, Prentice IC, Sitch S, Meyer R, Hooss G, Plattner GK, Gerber S, Hasselmann K (2001) Global warming feedbacks on terrestrial carbon uptake under the Intergovernmental Panel on Climate Change (IPCC) emission scenarios. Global Biogeochemical Cycles 15: 891–907
Jouzel J, Vimeux F, Caillon N, Delaygue G, Hoffmann G, Masson-Delmotte V, Parrenin F (2003) Magnitude of isotopics/temperature scaling for interpretation of central Antarctic ice cores. Journal of Geophysical Research 108(D12): 4361, doi: 10.1029/2002JD002677
Kaplan JO, Prentice IC, Knorr W, Valdes PJ (2002) Modeling the dynamics of terrestrial carbon storage since the Last Glacial Maximum. Geophysical Research Letters 29: 2074, doi: 10.1029/2002GL015230
Knutti R, Flückiger J, Stocker TF, Timmermann A (2004) Strong hemispheric coupling of glacial climate through continental freshwater discharge and ocean circulation. Nature 430: 851–856
Knutti R, Stocker TF, Wright DG (2000) The effects of subgrid-scale parametrizations in a zonally averaged ocean model. Journal of Physical Oceanography 30: 2738–2752
Köhler P, Fischer H (2004) Simulating changes in the terrestrial biosphere during the last glacial/interglacial transition. Global and Planetary Change 43: 33–55, doi: 10.1016/j.gloplacha.2004.02.005
Köhler P, Fischer H, Munhoven G, Zeebe RE (2005) Quantitative interpretation of atmospheric carbon records over the last glacial termination. Global Biogeochemical Cycles : in press, doi: 10.1029/2004GB002345
Körner C (2000) Biosphere responses to CO_2 enrichment. Ecological Applications 10: 1590–1619
Landais A, Caillon N, Goujon C, Grachev AM, Barnola JM, Chappellaz J, Jouzel J, Masson-Delmotte V, Leuenberger M (2004) Quantifi cation of rapid temperature change during DO event 12 and phasing with methane inferred from air isotopic measurements. Earth and Planetary Science Letters 225: 221–232
Lang C, Leuenberger M, Schwander J, Johnsen S (1999) 16°C rapid temperature variation in central Greenland 70,000 years ago. Science 286: 934–937
Leemans R, Cramer WP (1991) The IIASA climate database for land areas on a grid with 0.5^o resolution, vol. RR-91-18 of Research Reports. International Institute for Applied Systmes Analysis, Laxenburg, Austria
Lloyd J, Taylor JA (1994) On the temperature dependence of soil respiration. Functional Ecology 8: 315–323
Lucht W, Prentice IC, Myneni RB, Sitch S, Friedlingstein P, Cramer W, Bousquet P, Buermann W, Smith B (2002) Climatic control of the high-latitude vegetation greening trend and Pinatubo effect. Science 296: 1687–1689
Marchal O, Stocker TF, Joos F (1998) Impact of oceanic reorganizations on the ocean carbon cycle and atmospheric carbon dioxide content. Paleoceanography 13(3): 225–244
Marchal O, Stocker TF, Joos F (1999a) On large-scale physical and biogeochemical responses to abrupt changes in the Atlantic thermohaline circulation. In: PU Clark, RS Webb, LD Keigwin. (eds) Mechanisms of millennial-scale global climate change. , vol. 112 of Geophysical Monograph, American Geophysical Union, Washington, D.C., USA, pp. 263–284
Marchal O, Stocker TF, Joos F, Indermühle A, Blunier T, Tschumi J (1999b) Modelling the concentration of atmospheric CO_2 during the Younger Dryas climate event. Climate Dynamics 15: 341–354
McGuire AD, Sitch S, Dargaville R, Esser G, Foley J, Heimann M, Joos F, Kaplan J, Kicklighter DW, Meier RA, Melillo JM, Moore B, Prentice IC, Ramankutty N, Reichenau T, Schloss A, Tian H, Wittenberg U (2001) The effects of CO_2, climate and land-use on terrestrial carbon balance, 1920-1992: an analysis with four process-based ecosystem models. Global Biogeochemical Cycles 15: 183–206
McManus JF, Francois R, Gheradi JM, Keigwin LD, Brown-Leger S (2004) Collapse and rapid resumption of Atlantic meridional circulation linked to deglacial climate changes. Nature 428: 834–837
Meese DA, Gow A, Alley R, Zielinski G, Grootes P, Ram M, Taylor K, Mayewski P, Bolzan J (1997) The Greenland Ice Sheet Project 2 depth-age scale: Methods and results. Journal of Geophysical

Research 102: 26411–26423

Mikolajewicz U (1996) A meltwater-induced collapse of the 'conveyor belt' thermohaline circulation and its influence on the distribution of Δ^{14}C and δ^{18}O in the oceans, vol. 189 of Technical Report. Max Planck Institute for Meteorology, Hamburg, Germany

Monnin E, Indermühle A, Dällenbach A, Flückiger J, Stauffer B, Stocker TF, Raynaud D, Barnola JM (2001) Atmospheric CO_2 concentrations over the last glacial termination. Science 291: 112–114

Monnin E, Steig EJ, Siegenthaler U, Kawamura K, Schwander J, Stauffer B, Stocker TF, Morse DL, Barnola JM, Bellier B, Raynaud D, Fischer H (2004) Evidence for sustantial accumulation rate variability in Antarctica during the Holocene, through synchronization of CO_2 in the Taylor Dome, Dome C and DML ice cores. Earth and Planetary Science Letters 224: 45–54

Monteith JL (1995) Accomodation between transpiring vegetation and the convective boundary layer. Journal of Hydrology 166: 251–263

New M, Hulme M, Jones P (2000) Representing twentieth-century space-time climate variability: Development of 1901–95 monthly grids of terrestrial surface climate. Journal of Climate 13: 2217–2238

Oeschger H, Beer J, Siegenthaler U, Stauffer B (1984) Late glacial climate history from ice cores. In: JE Hansen, T Takahashi. (eds) Climate processes and climate sensitivity. , vol. 29 of Geophysical Monograph, American Geophysical Union, Washington, D.C., USA, pp. 299–306

Opsteegh JD, Haarsma RJ, Selten FM, Kattenberg A (1998) ECBILT: A dynamic alternative to mixed boundary conditions in ocean models. Tellus 50A: 348–367

Peltier WR (1994) Ice age paleotopography. Science 265: 195–201

Peteet D (1995) Global Younger Dryas? Quaternary International 28: 93–104

Pope VD, Gallani ML, Rowntree PR, Stratton RA (2000) The impact of new physical parametrizations in the Hadley Centre climate model: HadAM3. Climate Dynamics 16: 123–146

Prentice IC, Jolly D, participants B (2000) Mid-Holocene and glacial-maximum vegetation geography of northern continents and Africa. Journal of Biogeography 27: 507–519

Rashid H, Hesse R, Piper DJW (2003) Evidence for an additional Henrich event between H5 and H6 in the Labrador Sea. Paleoceanography 18: 1077, doi: 10.1029/2003PA000913

Röthlisberger R, Bigler M, Wolff EW, Monnin E, Joos F, Hutterli M (2004) Ice core evidence for the extent of past atmospheric CO_2 change due to iron fertilization. Geophysical Research Letters 31: L16207, doi: 10.1029/2004GL020338

Sabine CL, Heimann M, Artaxo P, Bakker DCE, Arthur CT, Field CB, Gruber N, Quéré CL, Prinn RG, Richey JE, Lankao PR, Sathaye JA, Valentini R (2004) Current status and past trends of the global carbon cycle. In: CB Field, MR Raupach. (eds) The global carbon cycle: integrating humans, climate, and the natural world. , Island Press, Washington, Covelo, London, pp. 17–44

Sarnthein M, Winn K, Jung SJA, Duplessy JC, Labeyrie L, Erlenkeuser H, Ganssen G (1994) Changes in East Atlantic deepwater circulation over the last 30,000 years: eight time slice reconstruction. Paleoceanography 99: 209–268

Scholze M (2003) Model studies on the response of the terrestrial carbon cycle to climate change and variability. Ph.D. thesis, Max Planck Institute for Meteorology, Hamburg, Germany

Scholze M, Kaplan JO, Knorr W, Heimann M (2003a) Climate and interannual variability of the atmosphere-biosphere $^{13}CO_2$ flux. Geophysical Research Letters 30: 1097, doi: 10.1029/2002GL015631

Scholze M, Knorr W, Heimann M (2003b) Modelling terrestrial vegetation dynamics and carbon cycling for an abrupt climate change event. The Holocene 13: 327–333

Siddall M, Rohling EJ, Almogi-Labin A, Hemleben C, Meischner D, Schmelzer I, Smeed DA (2003) Sea-level fluctuations during the last glacial cycle. Nature 423: 853–858

Siegenthaler U, Joos F (1992) Use of a simple model for studying oceanic tracer distributions and the global carbon cycle. Tellus 44B: 186–207

Sitch S (2000) The role of vegetation dynamics in the control of atmospheric CO_2 content. Ph.d. thesis, Department of Ecology, Lund University, Lund, Sweden

Sitch S, Smith B, Prentice IC, Arneth A, Bondeau A, Cramer W, O.Kaplan J, Lucht W, Sykes MT, Thonicke K, Venevsky S (2003) Evaluation of ecosystem dynamics, plant geography and terrestrial carbon cycling in the LPJ dynamic global vegetation model. Global Change Biology 9: 161–185

Skinner LC, Shackleton NJ (2004) Rapid transient changes in northeast Atlantic deep water ventilation age across Termination I. Paleoceanography 19: PA2005, doi: 10.1029/2003PA000983

Smith HJ, Fischer H, Wahlen M, Mastroianni D, Deck B (1999) Dual modes of the carbon cycle since the Last Glacial Maximum. Nature 400: 248–250

Stauffer B, Blunier T, Dällenbach A, Indermühle A, Schwander J, Stocker TF, Tschumi J, Chappellaz J, Raynaud D, Hammer CU, Claussen HB (1998) Atmospheric CO_2 concentration and millennial-scale climate change during the last glacial period. Nature 392: 59–62

Stenni B, Jouzel J, Masson-Delmotte V, Röthlisberger R, Castellano E, Cattani O, Falourd S, Johnsen SJ, Longinelli A, Sachs JP, Selmo E, Souchez R, Steffensen JP, Udisti R (2004) A late-glacial high-resolution site and source temperature record derived from the EPICA Dome C isotope records (East Antarctica). Earth and Planetary Science Letters 217: 183–195

Stocker TF (1998) The seesaw effect. Science 282: 61–62

Stocker TF, Johnsen SJ (2003) A minimum thermodynamic model for the bipolar seesaw. Paleoceanography 18: 1087, doi: 10.1029/2003PA000920

Thonicke K, Venevsky S, Sitch S, Cramer W (2001) The role of fire disturbance for global vegetation dynamics: coupling fire into a dynamic global vegetation model. Global Ecology and Biogeography 10: 661–677

Timmermann A, Gildor H, Schulz M, Tziperman E (2003) Coherent resonant millennial-scale climate oscillations triggered by massive meltwater pulses. Journal of Climate 16: 2569–2585

Timmermann A, Goosse H (2004) Is the wind stress forcing essential for the meridional overturing circulation? Geophysical Research Letters 31: L04303, doi: 10.1029/2003GL018777

Timmermann A, Justino F, Jin FF, Krebs U, Goosse H (2004) Surface temperature control in the north and tropical Pacific during the Last Glacial Maximum. Climate Dynamics 23: 353–370

Voelker AHL, workshop participants (2002) Global distribution of centennial-scale records for Marine Isotope Stage (MIS) 3: a database. Quaternary Science Reviews 21: 1185–1212

Table 1. The table shows the combination of observation-based data and model derived climate anomaly fields that were used to drive the LPJ-DGVM in different simulations.

Simulation	Data Set		
	Observations[1]	Output from ECBILT-CLIO[2]	Output from HadSM3[3]
		preindustrial simulations	
preindustrial control	yes	from ECBILT-CLIO control simulation	no
$F_{\square}$	yes	from ECBILT-CLIO freshwater simulation $F_{\square}$	no
$F_{\triangle}$	yes	from ECBILT-CLIO freshwater simulation $F_{\triangle}$	no
		simulations for past 21 kyr	
21 kyr to 6 kyr	yes	from ECBILT-CLIO freshwater simulation $F_{\square}$	from appropriate time slice simulation

1: Leemans and Cramer observation-based monthly mean climatologies (Leemans and Cramer, 1991) and interannual deviations from New et al. (2000) for temperature, precipiation and cloud cover. Interannual deviations are repeated in each 50 year simulation interval.
2: Time series of monthly anomalies in temperature and precipitation in response to NA THC changes from ECBILT-CLIO model. Anomalies with respect to the average monthly means of first 400 years of the ECBILT-CLIO control simulation were splined for each grid cell and calendar month using a 50-yr cut-off frequency to remove interannual variability.
3: Monthly anomalies in temperature, precipitation and cloud cover relative to preindustrial in response to millennial-scale changes in orbital parameters, greenhouse gas forcing and ice sheet extent from time slice experiments with HadSM3.

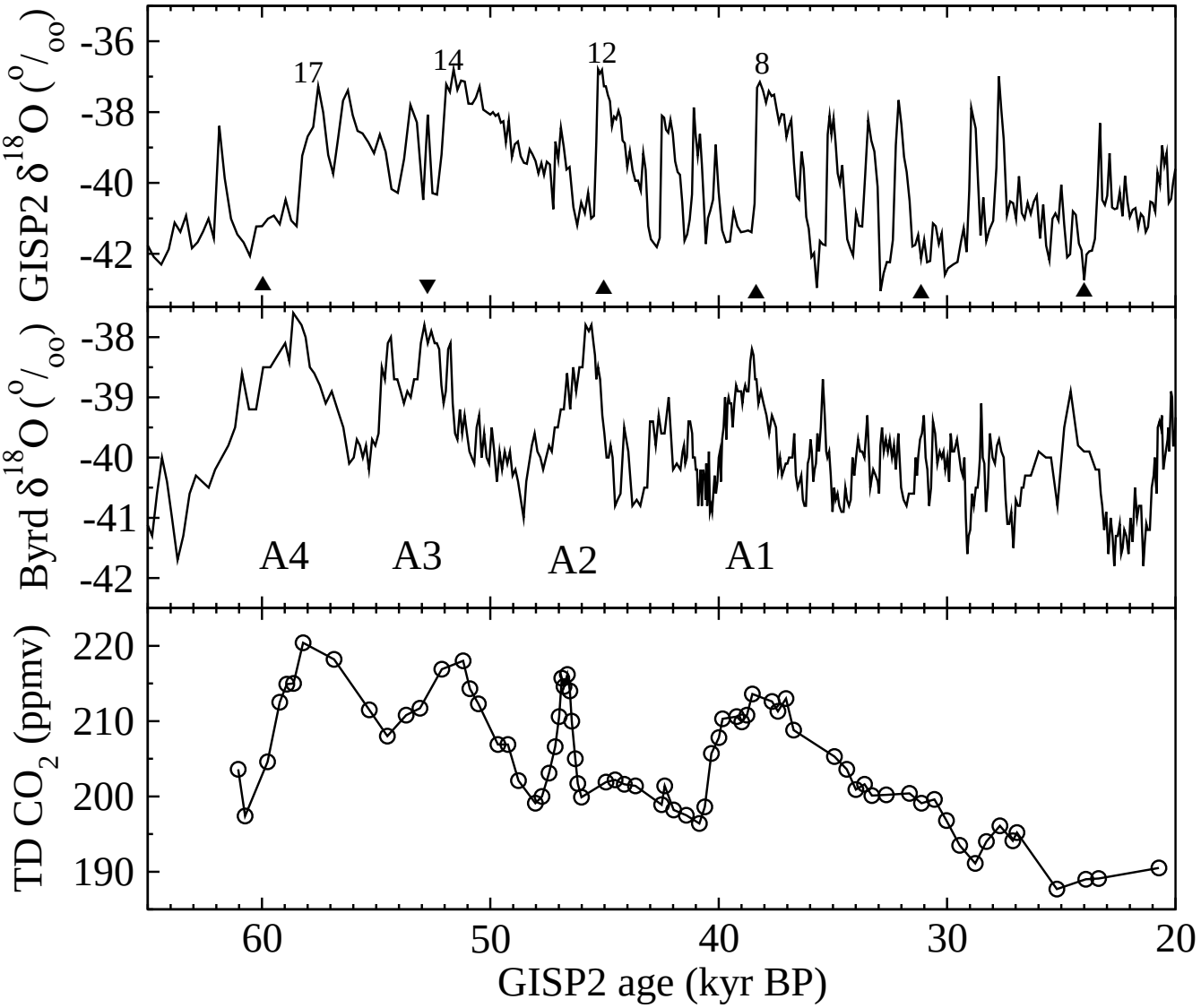

Fig. 1. Temporal evolution of CO_2 and high latitude temperatures (as seen in the isotopic thermometer of $\delta^{18}O$) between 65 and 20 kyr BP. North: GISP2 $\delta^{18}O$ (Grootes and Stuiver, 1997), South: Byrd $\delta^{18}O$ (Johnsen et al., 1972). Taylor Dome (TD) CO_2 (Indermühle et al., 2000). All data synchronised via CH_4 (Blunier et al., 1998; Brook et al., 1996, 2000; Blunier and Brook, 2001) on the GISP2 age scale (Meese et al., 1997). Triangles mark the timing of Heinrich events H6 – H2 (Hemming, 2004) and H5a (triangle upside down, Rashid et al., 2003), A1 – A4 label the Antarctic warm events. Major Dansgaard/Oeschger events 8, 12, 14, and 17 are also labelled.

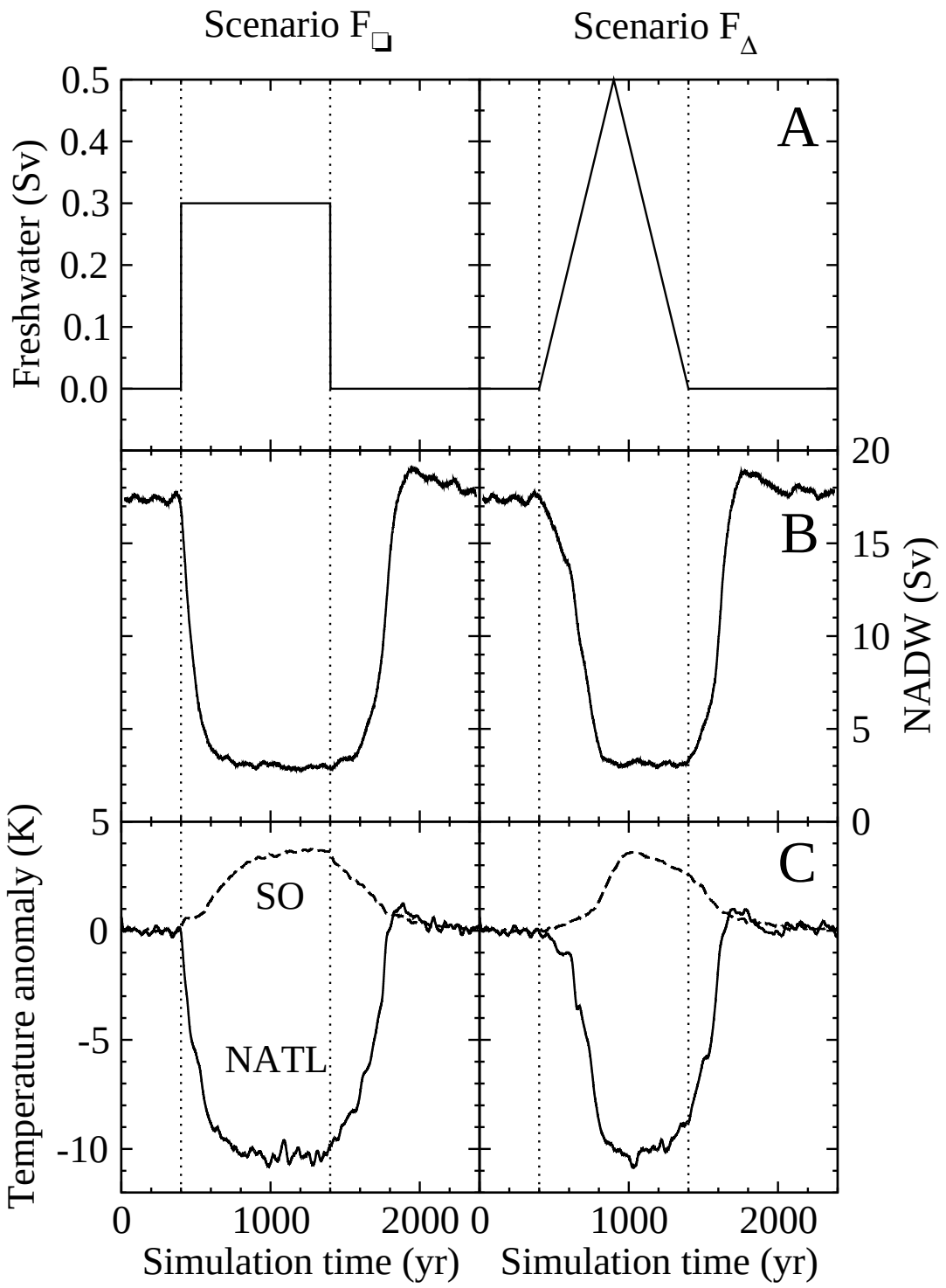

Fig. 2. Freshwater discharge into the North Atlantic (50°N-70°N) prescribed in simulations with the ECBILT-CLIO climate model (A), and the simulated change in North Atlantic Deep Water (NADW) exported at 30°S (B) and in near surface air temperature of the whole North Atlantic region (NATL, 60°W-20°E, 50°N-80°N), and the Southern Ocean (SO, 65°S-50°S) (C) for scenario $F_\square$ (left) and $F_\triangle$ (right).

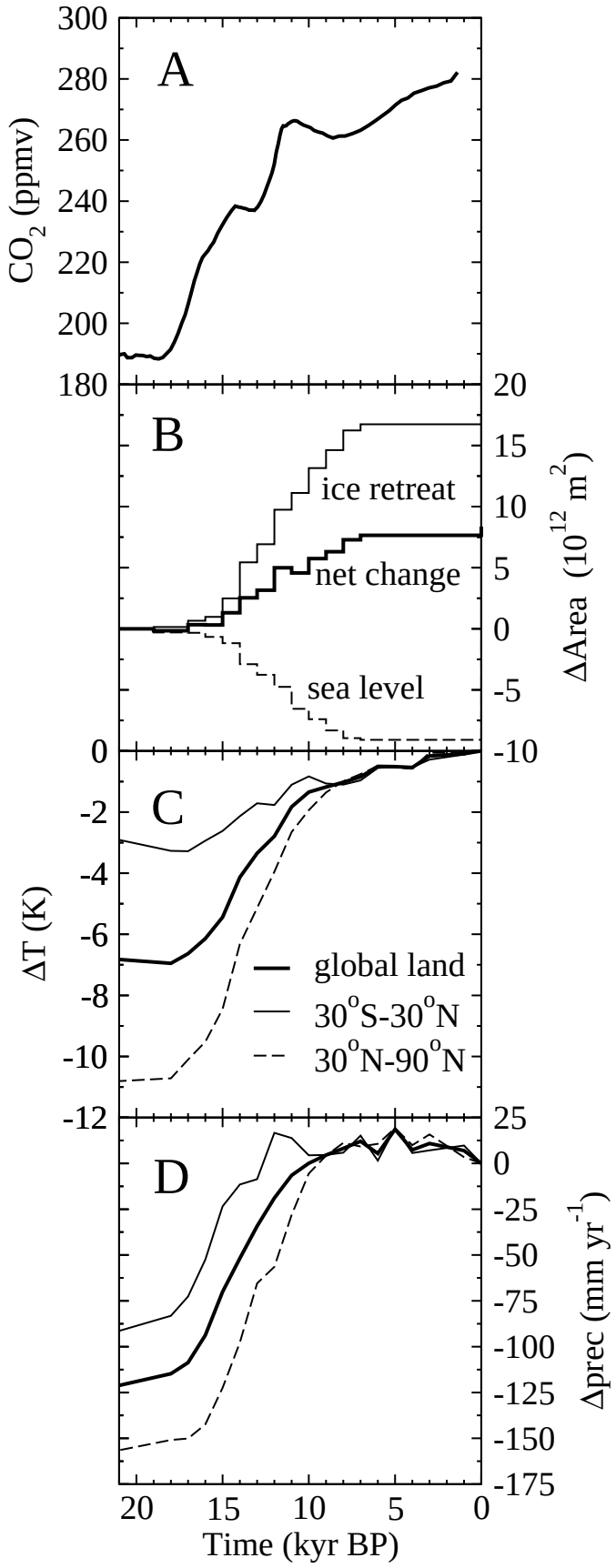

Fig. 3. Changes in climate boundary conditions over the past 21 kyr. A: CO_2 from EPICA Dome C (Monnin et al., 2001) synchronised via CH_4 to the GISP2 age scale and splined (Köhler et al., 2005). B: Changes in land available for plant growth relative to 21 kyr BP in response to ice sheet retreat and sea level rise and the resulting net change (Peltier, 1994). C, D: Temperature and precipitation anomalies over land area (excluding Antarctica) as simulated with the Hadley Centre HadSM3 climate model for time slice experiments about every 1 kyr and linear interpolation between them, globally averaged and for different latitudinal bands (sub-fi gures B, C, D adapted from Joos et al., 2004)

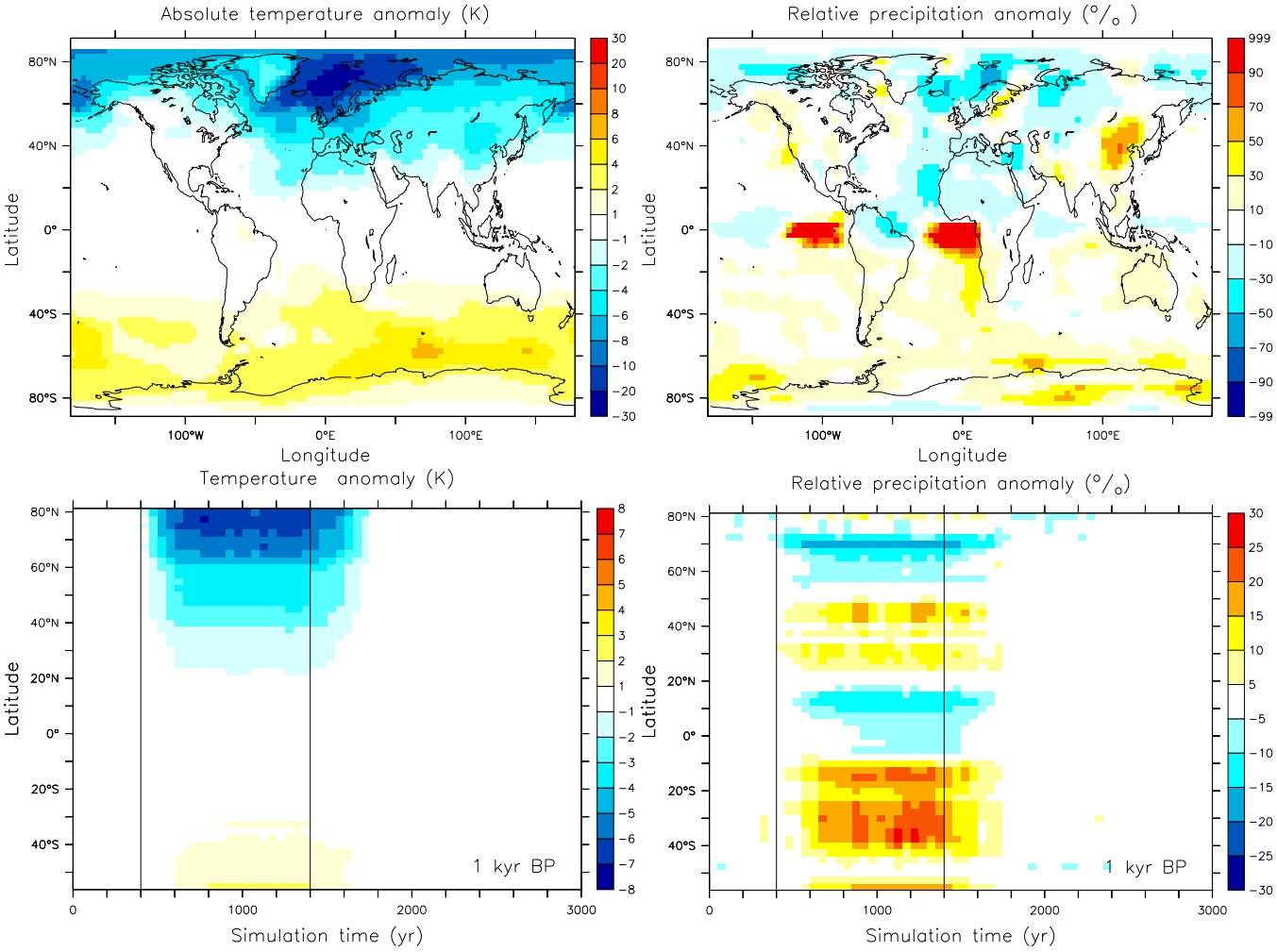

Fig. 4. Temperature and precipitation anomalies for the freshwater experiment $F_{\square}$. Top: Calculated for $t = 1001 - 1200$ yr of the simulation period. Bottom: Zonally-averaged absolute temperature and relative precipitation anomalies over non-glaciated land versus time for preindustrial conditions ($t = 1$ kyr BP). Anomalies were calculated with respect to the temporal averages of the first 400 yr of the simulation. Vertical lines indicate the start and end of the prescribed freshwater discharge.

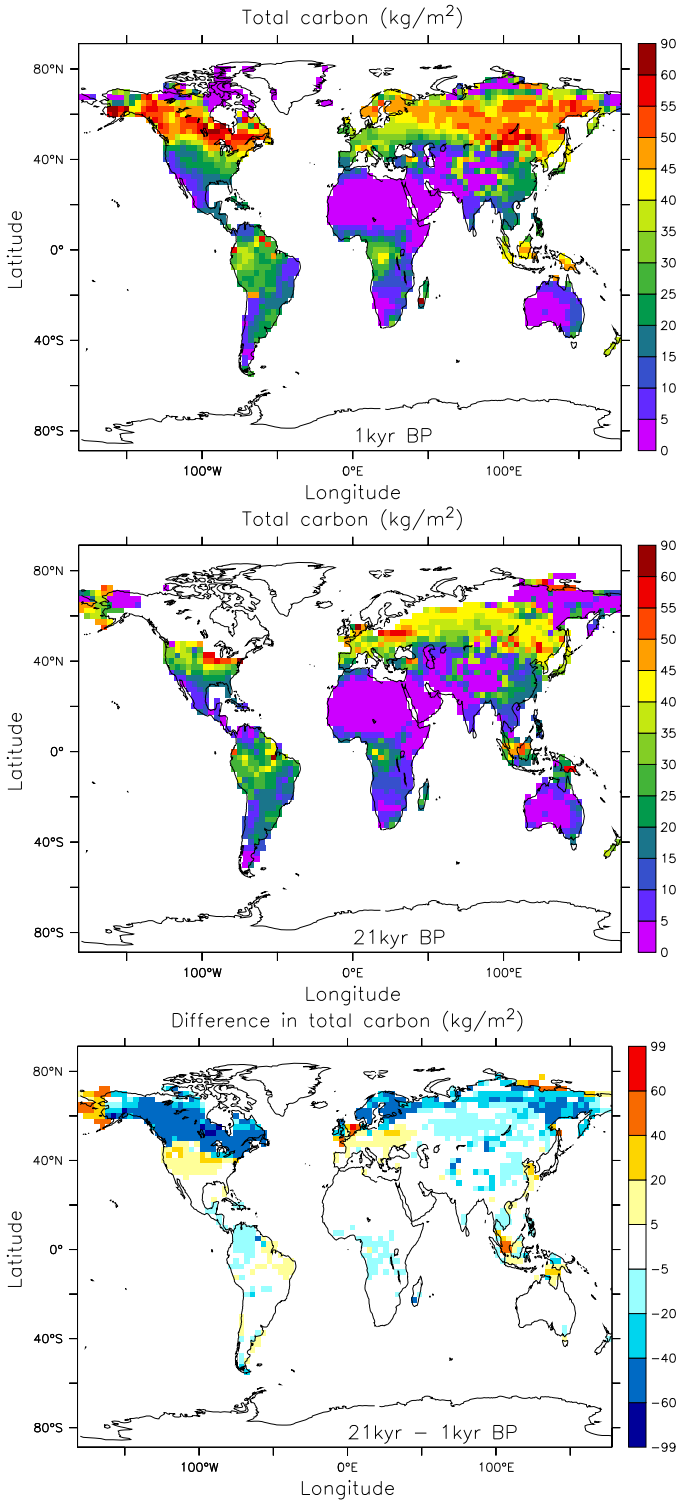

Fig. 5. Total terrestrial carbon storage simulated with the LPJ-DGVM for preindustrial boundary conditions ($t = 1$ kyr BP) (top) and Last Glacial Maximum conditions ($t = 21$ kyr BP) (middle) and their difference (LGM minus preindustrial) (bottom). The present-day land distribution is shown by solid lines.

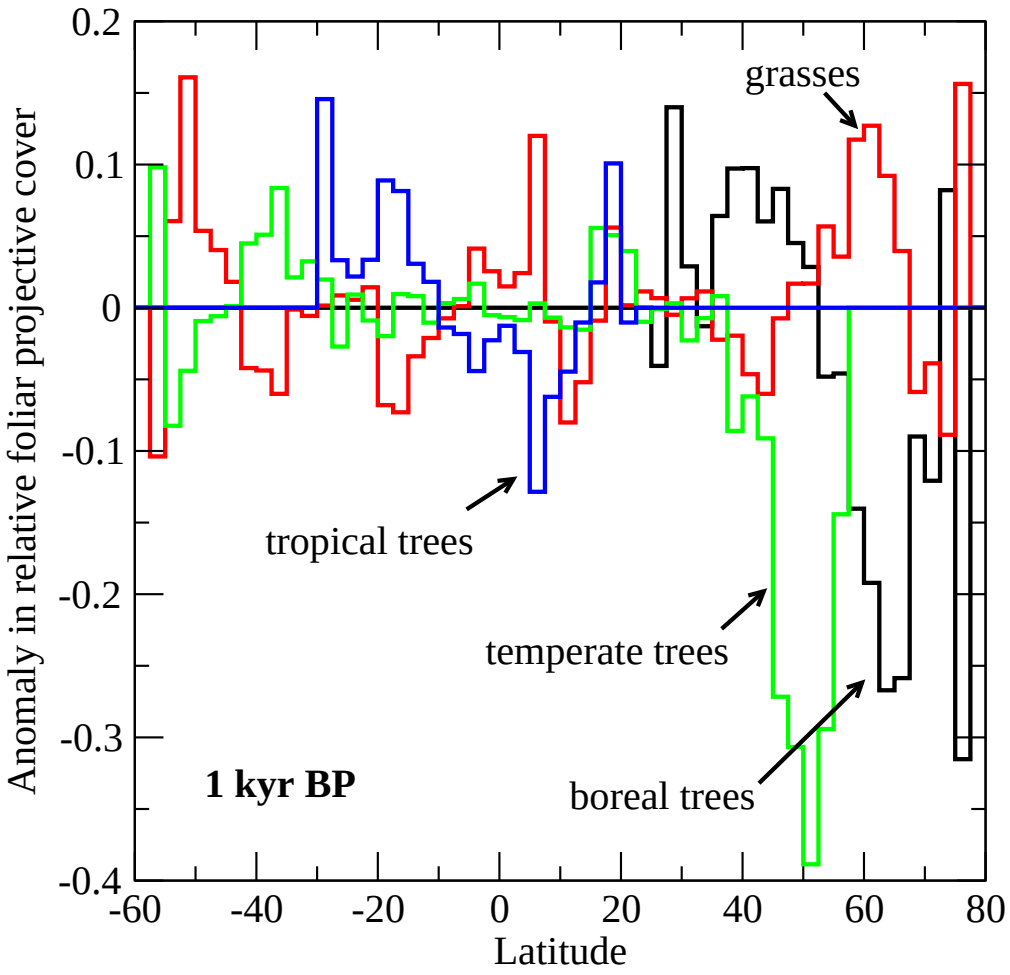

Fig. 6. Anomalies in the relative foliar protective cover of tropical, temperate, and boreal trees and grasses for scenario $F_{\square}$ and preindustrial initial conditions (1 kyr BP). The anomaly is calculated as average distribution during the peak cold phase ($t = 1001 - 1400$ yr) with respect to the first 400 yr of the simulation, i.e. before the start of the freshwater discharge in ECBILT-CLIO. These model results are largely independent of CO_2 fertilisation feedbacks. Results shown are from simulations without CO_2 fertilisation feedbacks.

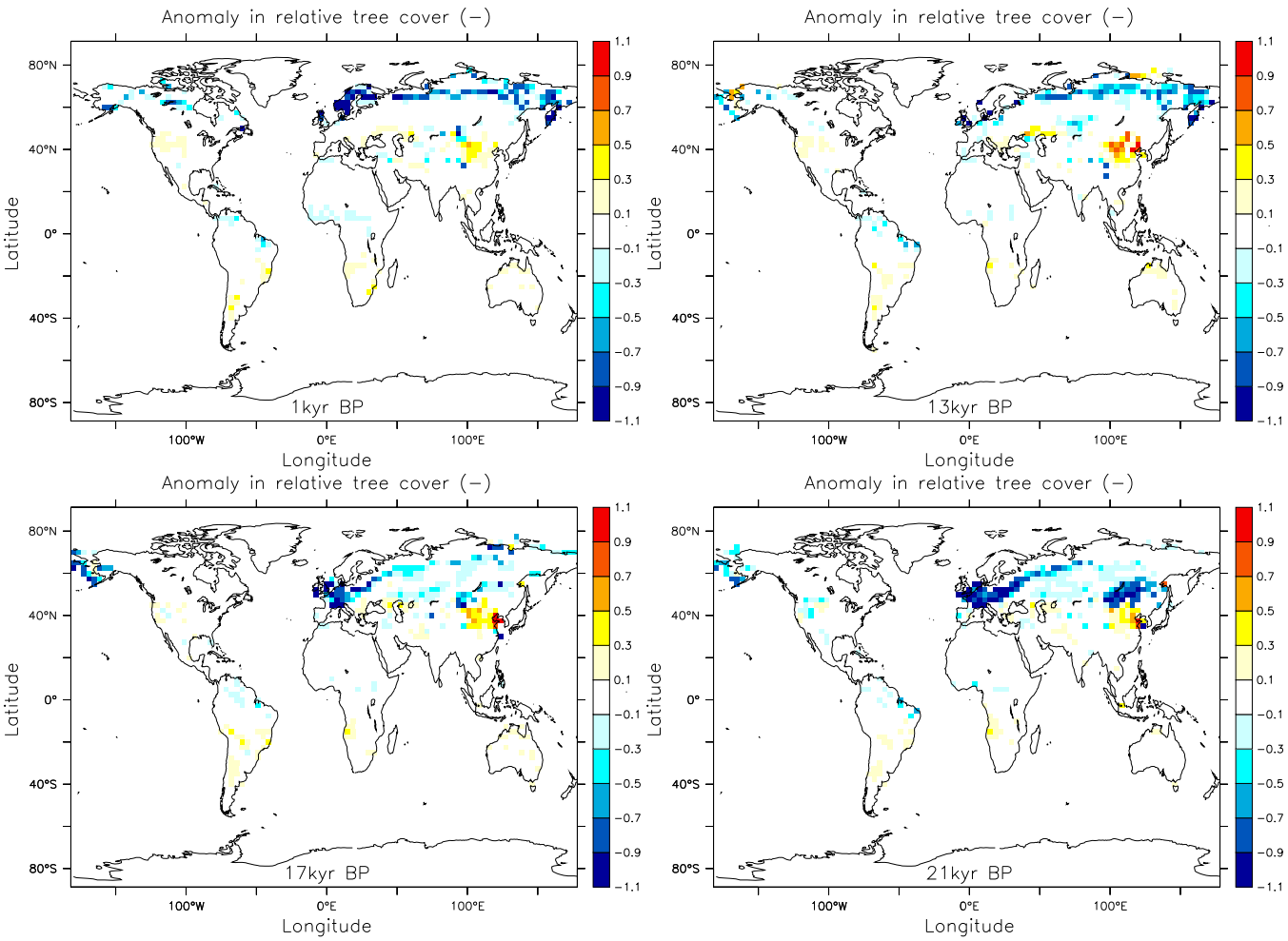

Fig. 7. Anomalies in the relative tree cover for scenario $F_{\square}$ and different initial conditions (t =1, 13, 17, and 21 kyr BP). The anomaly is calculated as average distribution during the peak cold phase ($t = 1001 - 1400$ yr) with respect to the first 400 yr of the simulation, i.e. before the start of the freshwater discharge in ECBILT-CLIO. These model results are largely independent of CO_2 fertilisation feedbacks. Results shown are from simulations without CO_2 fertilisation feedbacks. Blue colours indicate a loss of relative tree coverage and yellow-red colours a gain relative to the average of the first 400 yr.

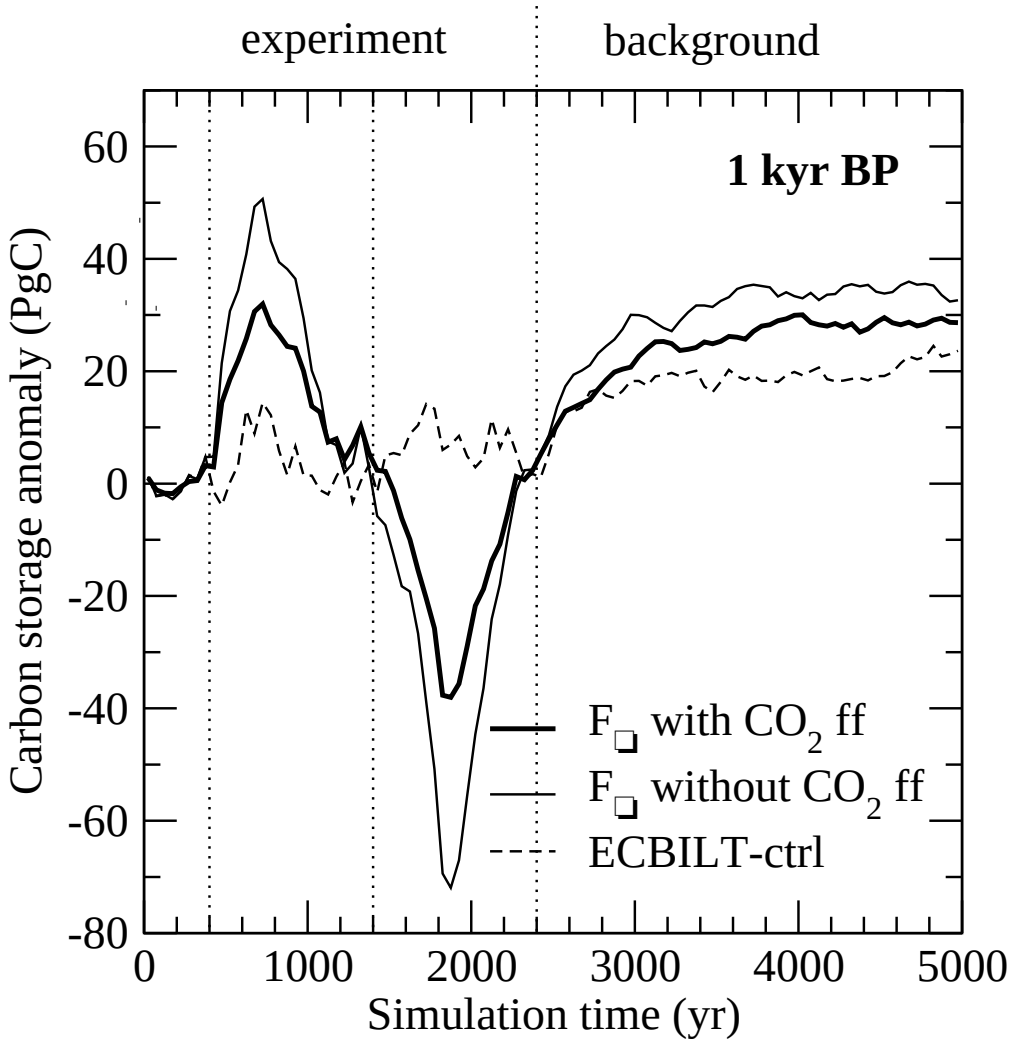

Fig. 8. Change in global terrestrial carbon storage versus time simulated by the LPJ-DGVM in response to the climate perturbations of the ECBILT-CLIO freshwater experiment $F_{\square}$ (Fig. 2) and preindustrial (1 kyr BP) initial conditions. Results are shown for experiments with (solid) and without (thin) CO_2 fertilisation feedbacks (ff) and for a control (dash) without freshwater discharge and without CO_2 fertilisation feedbacks. Vertical lines at 400 yr and 1400 yr indicate the beginning and the end of the freshwater discharge in ECBILT-CLIO. After year 2400 the LPJ-DGVM was again forced with the initial climate conditions.

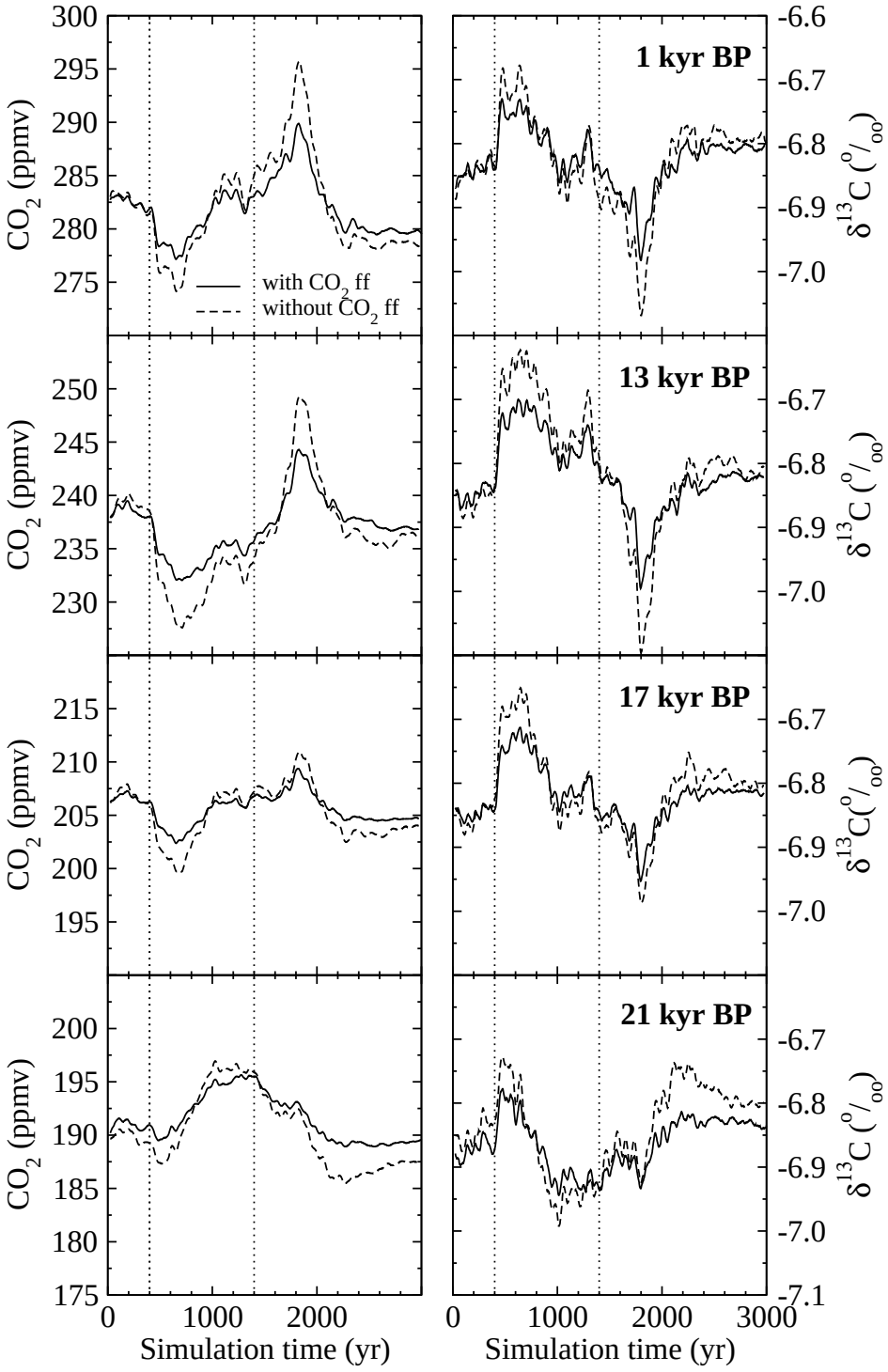

Fig. 9. Anomalies in atmospheric CO_2 (left) and $\delta^{13}C$ (right) for different initial conditions ($t = 1, 13, 17$, and 21 kyr BP) as simulated with the LPJ-DGVM in response to the scenario $F_{\square}$ and for simulations with (solid) and without (dash) CO_2 fertilisation feedbacks (ff). Vertical lines at 400 yr and 1400 yr indicate the beginning and the end of the freshwater discharge.

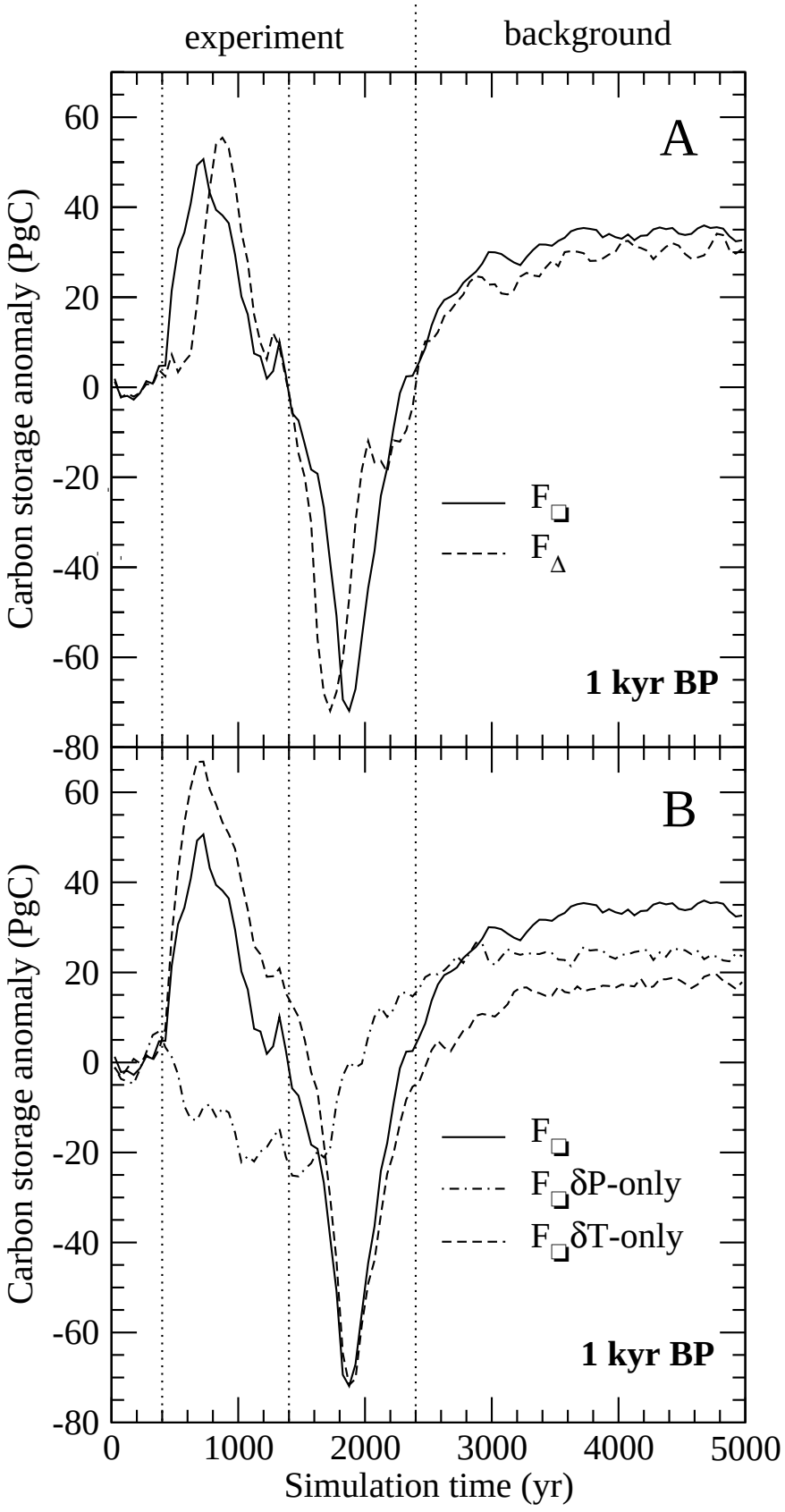

Fig. 10. Sensitivity of modelled changes in global terrestrial carbon storage to (A) the form of the freshwater scenario ($F_{\square}$: solid; F_{Δ}: dash) and to (B) individual climatic drivers for simulations without CO_2 fertilisation feedbacks and for preindustrial boundary conditions ($t = 1$ kyr BP). Only ECBILT-CLIO temperature anomalies have been applied in experiment $F_{\square}\delta$T-only (dash), whereas precipitation fi elds were from the control run. Only precipitation anomalies have been applied in experiment $F_{\square}\delta$P-only (dash-dot). Vertical lines at 400 yr and 1400 yr indicate the beginning and the end of the freshwater discharge in ECBILT-CLIO.

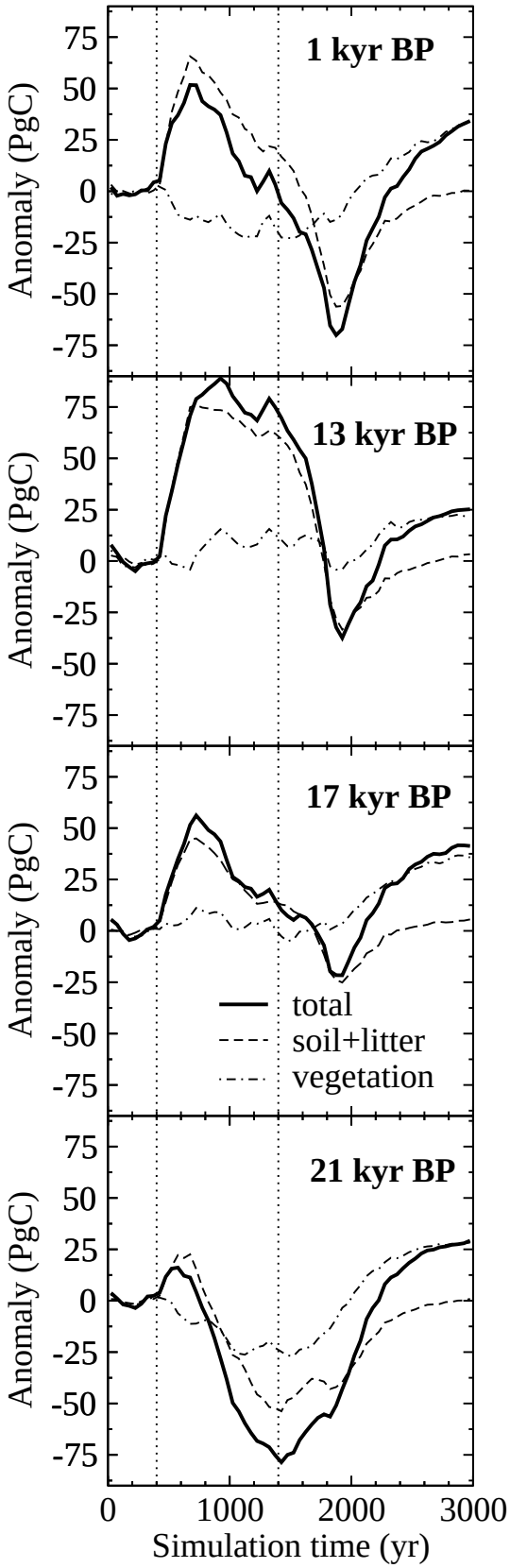

Fig. 11. Anomalies in the amount of carbon stored globally in soil and litter (dash), vegetation (dash-dot) and their total (solid) for different initial conditions ($t = 1, 13, 17,$ and 21 kyr BP) as simulated with the LPJ-DGVM in response to the scenario $F_{\square}$ and without CO_2 fertilisation feedbacks. Vertical lines at 400 yr and 1400 yr indicate the beginning and the end of the freshwater discharge in ECBILT-CLIO.

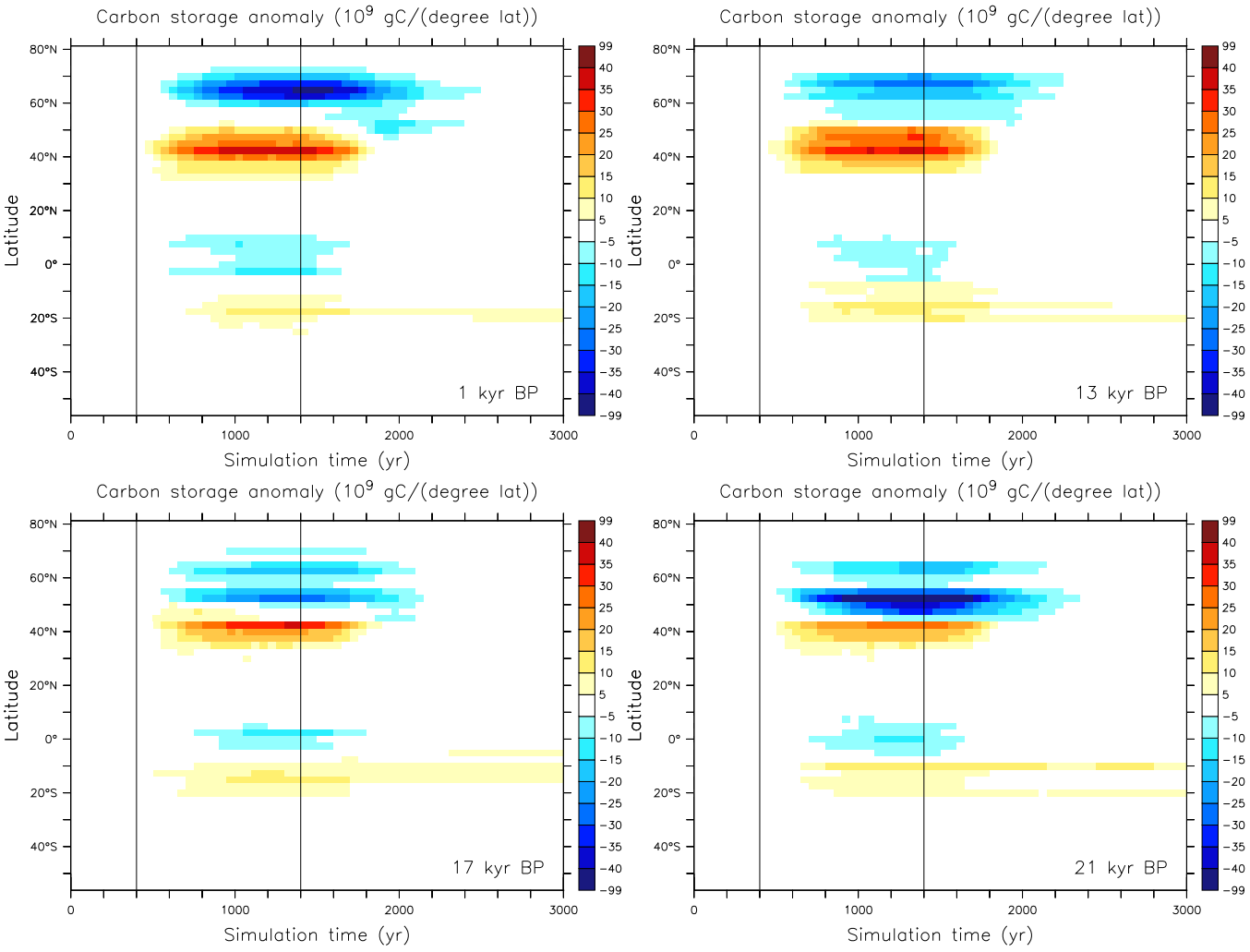

Fig. 12. Zonally-averaged anomalies in total land carbon storage versus time for different initial conditions ($t = 1, 13, 17$, and 21 kyr BP) as simulated by the LPJ-DGVM under constant CO_2 (no CO_2 fertilisation feedbacks) and using ECBILT-CLIO climate anomalies from experiment $F_{\square}$. Vertical lines at 400 yr and 1400 yr indicate the beginning and the end of the freshwater discharge in ECBILT-CLIO. Blue colours indicate a loss of carbon and yellow-red colours a gain of carbon relative to the average of the first 400 yr.

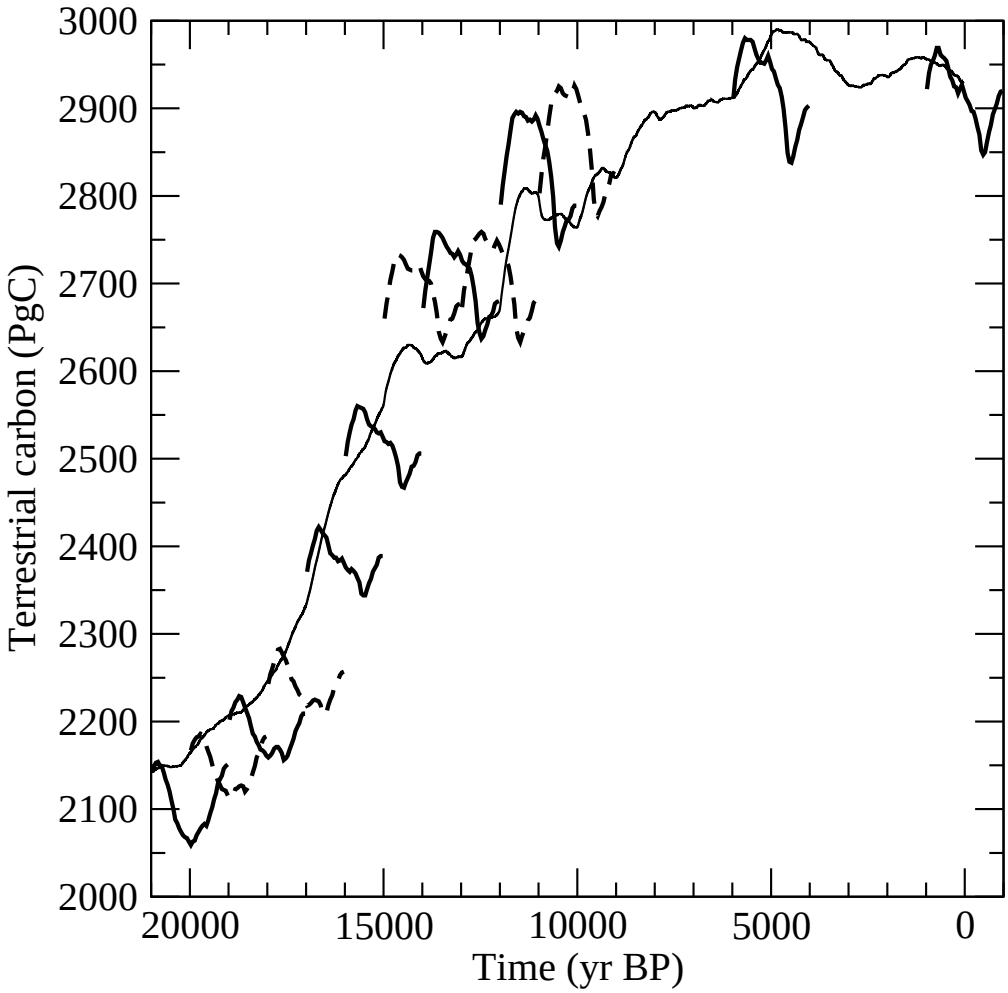

Fig. 13. Change in global terrestrial carbon storage versus time simulated with the LPJ-DGVM in response to the climate perturbations of the ECBILT-CLIO freshwater experiment $F_{\square}$ for a range of initial conditions (thick lines, dashed and solid to allow the perception of different neighbouring experiments). Plotted are results after the start of the freshwater discharge (simulation year 400). For each experiment, the LPJ-DGVM has been spun-up to equilibrium under the background climate conditions obtained from time slice simulations with the Hadley Centre climate model, atmospheric CO_2, and ice sheet extent as representative for a particular time of the past 21 kyr. Ice sheet extent and CO_2 has been kept constant. The thin line shows the evolution of terrestrial carbon storage over the past 21 kyr as simulated by forcing the LPJ-DGVM with a transient climate evolution from the Hadley Centre model, and changing boundary conditions of sea level, land ice sheets and CO_2. Carbon is transferred to the atmosphere once a grid area is either fboded or overrun by growing ice sheets with an e-folding time of 100 years.

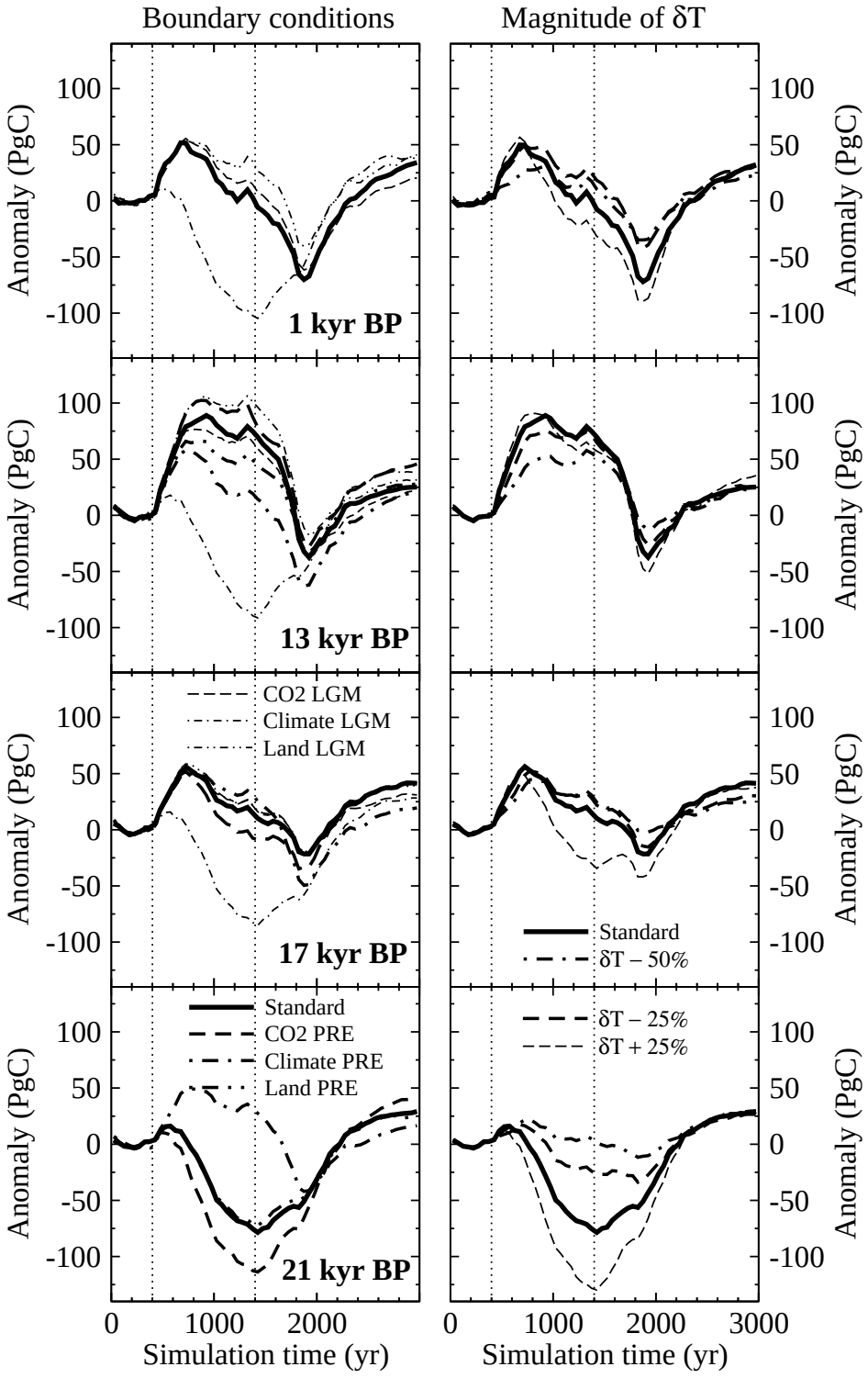

Fig. 14. Sensitivity of modelled changes in global terrestrial carbon storage to individual climatic drivers defi ning the initial climate state (left) and to the magnitude of the ECBILT-CLIO temperature anomalies (right) for simulations without CO_2 fertilisation feedbacks and for a range of initial conditions (1, 13, 17, and 21 kyr BP). CO_2 (dash), initial temperature and precipitation fi elds (dash-dot), and the land mask (dash-dot-dot) were set individually to either preindustrial (bold) or LGM (thin) conditions during the LPJ-DGVM spin-up and freshwater experiment, whereas the other drivers were kept at values that correspond to the starting time of the simulation. The magnitude of the temperature anomaly as calculated by ECBILT-CLIO was varied by $+25\%$ (thin dash), -25% (bold dash) and -50% (bold dash-dot). Vertical lines at 400 yr and 1400 yr indicate the beginning and the end of the freshwater discharge.